Ultrahigh-energy cosmic-ray spectrum

Christopher T. Hill
Fermi National Accelerator Laboratory, P.O. Box 500, Batavia, Illinois 60510

David N. Schramm
The University of Chicago, Chicago, Illinois 60637
and Fermi National Accelerator Laboratory, P.O. Box 500, Batavia, Illinois 60510
(Received 24 February 1984)

We analyze the evolution of the ultrahigh-energy cosmic-ray spectrum upon traversing the 2.7 °K microwave background with respect to pion photoproduction, pair-production reactions, and cosmological effects. Our approach employs exact transport equations which manifestly conserve nucleon number and embody the laboratory details of these reactions. A spectrum enhancement appears around 6×10^{19} eV due to the "pile-up" of energy-degraded nucleons, and a "dip" occurs around 10^{19} eV due to combined effects. Both of these features appear in the observational spectrum. We analyze the resulting neutrino spectrum and the effects of cosmological source distributions. We present a complete model of the ultrahigh-energy spectrum and anisotropy in reasonable agreement with observation and which predicts an observable electron-neutrino spectrum.

I. INTRODUCTION

Shortly after the discovery of the 2.7 °K microwave background radiation it was suggested that there must exist a fundamental cutoff in the ultrahigh-energy cosmic-ray spectrum.[1,2] A nucleon of energy exceeding 10^{20} eV colliding head-on with a typical 2.7 °K photon comprises a system of sufficient total center-of-mass energy to produce pions by the photoproduction reaction. The energy loss of the nucleon is a significant fraction of the incident energy. Moreover, the pion-photoproduction cross section is quite large immediately above threshold due to resonance production, rising quickly to 500 mb for γ laboratory energies of order 0.3 GeV, and settling down asymptotically to roughly ~ 120 mb for energies exceeding a few GeV. Thus, if the ultrahigh-energy cosmic rays are produced in distant extragalactic sources, then the observed spectrum must be cut off at an energy scale of order 10^{20} eV. In fact, if the sources are more than a few interaction lengths away, then collisions with photons in the high-energy Boltzmann tail of the 2.7 °K photon distribution will reduce the onset of the cutoff to about 5×10^{19} eV.

It is widely believed that cosmic rays of energies exceeding 10^{15} eV begin to leak out of the galactic confining magnetic field. At this energy scale we encounter the so-called "knee" in the observed spectrum, which steepens from a differential index of 2.5 below 10^{15} eV to ~ 3 above, and which has been attributed to a magnetic deconfinement effect.[3,4] An observer inside of the galaxy sees, therefore, a spectrum behaving like $j_0(E)t(E)\propto 1/E^{2.5}$, steepening to $1/E^{3.0}$ for $E>10^{15}$ eV. Here, $t(E)$ is an effective trapping time due to diffusion in the galactic magnetic field which can decrease more rapidly with energy above 10^{15} eV, giving rise to the knee structure. If we discount the cosmic rays produced in other galaxies, we might expect that the steep part of the spectrum continues until a "line of sight" or "prompt" component is reached from local galactic events. This might be argued to be the source of the "ankle" at energies above 10^{19} eV. The difficulty here is that the reported corollary anisotropy is directed normal to the galactic plane (in the general direction of the Virgo cluster).[5] One might argue that the iron-rich spectrum could be steered by the galactic B field to produce such an effect.[6] However, this mechanism may be difficult to implement in the known geometry of the galactic B field.[6] Furthermore, the prompt component of the spectrum should not be iron rich, since it is not subject to the trapping-time effect, and it should contain mostly protons and even neutrons. Thus the anisotropy becomes hard to understand; in fact, the presence of a pinpoint image of the source in the general direction of the galactic plane would be expected.

We suppose that there will occur some energy scale E_c at which the local spectrum becomes comparable to or less than the cosmological component. We shall refer to E_c as the "crossover" energy, and the above estimate suggests that crossover must occur near the knee in the spectrum, $10^{(15\text{ to }16)}$ eV. Of course, the existence of the crossover depends upon the extent to which the local spectrum steepens by leakage, the steeping effects which may be present in the cosmological spectrum, and the overall normalizations. In fact, we shall find that there must exist some steepening of the cosmological spectrum due to cosmological red-shift effects, a point originally emphasized by Hillas.[7] We emphasize that it is not known definitively whether the cosmic rays above 10^{15} eV are local, extragalactic, or both. One of our objectives, at present is to improve substantially the predictions of the cosmological model.

It is then natural to associate the ankle structure either with the crossover energy, or with the presence of a particularly bright extragalactic, though relatively nearby source, superimposed on a cosmological diffuse background, or both. This then fixes the normalization of the

extragalactic component, and allows us to make quantitative estimates of the neutrino yields, and spectrum structure as arise by photoproduction.

Such mechanisms for the spectrum above the knee have been previously discussed.[4,7,8,9] Hillas[7] has argued that the structure of the spectrum between 10^{15} eV and 10^{19} eV can be understood as a cosmological evolution due to red-shift effects from sources most active at large red-shift, e.g., $z \gtrsim 30$ to the present. Blumenthal[9] has done a quantitative analysis of the effects of pair-production interactions (e^+e^- pair creation on nucleons by 2.7°K photons with higher energies at large red-shift) in a Hillas model and finds a reasonable agreement with a $1/E^3$ observed spectrum up to 10^{19} eV by assuming a flatter $1/E^{2.5}$ injection spectrum, increasing activity proportional to $(1+z)^4$, and integrating back to $z \sim 15$ to 50. (There is even a slight vestige of a flattening in Blumenthal's spectrum at 10^{19} eV.) These analyses have, however, failed to describe the ankle structure due to the treatment of photomeson production. These analyses also implicitly assume the crossover energy to be about 10^{16} eV.

However, in Sec. V we will show that the occurrence of the general ankle structure in models with $1/E^{2.0\pm0.5}$ injection spectra are in good agreement with observation when the spectrum evolution is properly treated. We also require an assumption of proximity to the Virgo cluster, relative to the nearest typical diffuse sources, in order to accommodate the anisotropy and events reported above 10^{20} eV. We will obtain an unambiguous prediction for the neutrino and photon spectra, which should be experimentally verifiable.

A new feature which emerges in our analysis and which has not been previously discussed in the literature is the appearance of a "dip" in E^3dN/dE at about 10^{19} eV. This dip appears in the published data and is statistically significant. We feel it lends potentially strong support to the analysis presented here and to the idea of long-range propagation (>100 Mpc).

If the spectrum above 10^{19} eV is extragalactic in origin then it is predominantly composed of nucleons. Nuclei are expected to have substantially broken apart by photoreactions with starlight and the 2.7°K background photons.[1,10] We remark that even free neutrons with energy in the range 10^{19} to 10^{20} eV can travel distances of order (few) Mp before β decay due to time dilation. Photomeson production reactions will involve neutrons, and the appropriate averaging over isospin must be included. We shall thus approximate the ultrahigh-energy cosmic rays as an average over nucleons (and antinucleons) in the evolution of the spectrum. The production of e^+e^- pairs is extremely important and is also considered. Although the cross section for this process is roughly 3 to 4 orders of magnitude larger than that of photomeson production, the energy loss per nucleon is correspondingly 6 orders of magnitude smaller. This is an extremely important effect cosmologically for nucleons that have traversed a distance of order a tenth of the present horizon radius (this need be only the total path length traversed, and need not be the total range of the particle due to magnetic localization on a supercluster scale). We shall not follow the produced e^+e^- pairs which rapidly lose energy by Compton scattering on the 2.7°K photons[11] and by synchrotron energy loss in the intergalactic magnetic field. Correspondingly, there will develop a high-energy γ component, and the appropriate transport equation describing these components must allow for the mixing of γ's to pairs and vice versa.[12] These are extremely important potential corollary observables which should be analyzed in detail, as we have at present for the induced neutrino spectrum.

Observationally, there is a controversial development in the ultrahigh-energy cosmic-ray spectrum which onsets at about 3×10^{19} eV. Here some groups report a general flattening of the spectrum from a differential index of order 3.0 to about 2.5 (Refs. 13 and 14). Also, there are a large number of events reported with energies exceeding 10^{20} eV (Refs. 13 and 14). This is seemingly very difficult to understand in terms of the conventional Greisen-Zatsepin cutoff with extragalactic sources. On the contrary, the Yakutsk group after previously claiming to have seen the effect now reports no flattening of the spectrum at these energies[15] and results generally consistent with the expectation of a cutoff. Although the reported flattening derives from significantly more data, the Yakutsk data involves greater redundancy in energy calibration. The ankle may or may not be seen by the southern-hemisphere group.[16] However, Yakutsk also fails to see the dramatic anisotropy reported by the Haverah Park group,[4,5,17] and it is difficult to understand this discrepancy which is less immune to the problems of energy calibration. Furthermore, a recent comparative analysis of the electromagnetic calibration of the Haverah Park array and the Yakutsk array shows that they are generally consistent,[18] compounding the mystery of the discrepancy. The resolution of this dilemma will perhaps await better statistics and more data involving greater-integrated-density measurements.

It is in part due to this interesting and exciting controversy that we have undertaken to reanalyze the Greisen-Zatsepin cutoff in the more reliable framework of transport equations. Given a final verdict on the observational situation, what can we hope to learn about the underlying mechanisms? Also, given the present observational situation can we begin to glimpse a complete picture of the sources, origins, and evolutionary effects inherent in the ultrahigh-energy (UHE) cosmic rays? In the present paper, we argue from the vantage point of an improved evolutionary analysis that the UHE spectrum is indeed beginning to form a consistent picture.

In the present paper we will reexamine the expectations for the structure of the cosmic-ray spectrum at ultrahigh energies (see Ref. 19). Our method will differ from those of preceding authors in a significant way. Instead of the mean-interaction-length and energy-loss approximations used in preceding analyses,[1,2,8,20] we will employ statistically exact transport equations which incorporate the laboratory details of photoproduction and meson decays. An important aspect of our analysis is the explicit conservation of baryon number which leads to an "active recoil nucleon" and the collision processes are iterated until the recoil particles drop effectively below threshold to participate in further interactions. This leads to an effective

multiplier in the number of secondary photons and neutrinos that are produced since one nucleon can experience several collisions in this cascade process.

We find that an enhancement always occurs before the Greisen-Zatsepin (GZ) cutoff as a consequence of the pile-up of energy-degraded nucleons recoiling down from higher energies and ending up approximately below threshold to undergo further photoproduction reactions, of order 5×10^{19} eV. The shape of the enhancement is essentially "universal" in the sense that after a few interaction lengths it is very weakly dependent upon the input spectrum shape, but does depend strongly upon the input spectrum normalization. This is reminiscent of a "fixed-point" behavior. In fact, we find that the spectrum above 10^{18} eV can be understood completely in terms of an injection spectrum of order $1/E^{2.0\pm0.5}$ which is steepened by the various cumulative effects and interactions into a $1/E^3$ form up to 3×10^{19} eV, and we can accommodate, by including a "local" or exceptionally bright source, e.g., the Virgo supercluster, a large ankle structure extending up to 10^{20} eV. This model can incorporate, but does not require, a Hillas-Blumenthal model for the spectrum from 10^{15} eV to 10^{18} eV or a magnetic confinement-leakage model. In spirit this is a model quite similar to that discussed previously by Giler, Strong, Wdowcyzk, and Wolfendale,[8] but differs substantially in details and results.

This model leads to an umambiguous prediction for the neutrino spectrum. In particular, even though we consider arbitrary injection indices and bright phase exponents in treating the cosmological-source sums we find that the UHE neutrino spectrum always has a slope equal to the observed cosmic-ray slope plus $\frac{1}{2}$. Other features of the neutrino spectrum emerge which contain detailed information about the "bright phase."

The important phenomena of secondary photons and neutrinos have been proposed and analyzed by previous authors, most notably Stecker.[2,20] However, these analyses again neglect the recoil proton that emerges from the initial collision, while retaining most of the incident energy and which can initiate subsequent collisions. Thus, the spectrum of produced secondaries has a normalization which is related to the pile-up normalization, but is significantly larger than that obtained previously. We will also find that our numerical evolution leads to a smaller cutoff energy in the neutrino and photon spectra than those obtained previously. We find an effective cutoff of order 2×10^{19} eV. We will obtain a noncosmologically sensitive lower limit of about $1/\mathrm{km}^2\mathrm{yr\,sr}$ integrated neutrino flux above 10^{18} eV, and results roughly $100\times$ greater with reasonable bright-phase models. These latter results approach detectability in the Fly's Eye within a factor of 10 to 100 (Ref. 21). The prediction depends only upon the assumption of increasing cosmic-ray activity back to redshifts greater than 3 and that the UHE cosmic rays are extragalactic nucleons. Measuring the neutrino spectrum to lower energies than 10^{18} eV would determine the redshift of maximum cosmic-ray luminosity.

Our paper is organized as follows. We begin in Sec. III by constructing the spectrum evolution transport equation. We introduce rescaled variables that describe the kinematics in the cosmic-ray laboratory frame (CRLF) and which are employed in our numerical-integration routine. We briefly review photoproduction data at low energies and describe some fits which we employ in our analysis. In the CRLF we obtain convenient parametrizations of the recoil nucleon and produced pion energy spectra in terms of our scaling variables. We briefly describe our numerical-integration routine COSEV. In Sec. III we discuss in detail the cosmological effects and develop a general formalism. We discuss here the somewhat nontrivial question of normalization of the diffuse relative to the local components of the nucleon and neutrino spectra. In Sec. IV we present the results of several numerical analyses for various assumed input spectra. We consider pointlike and cosmological source distributions, for which the pair production process (e^+e^- pair production) plays an important role. In Sec. V we present a complete model of the UHE cosmic-ray spectrum which appears to be in good agreement with the observational data. Upon first reading we might suggest that one skip directly to Secs. IV and V. We present a brief summary and conclusions in Sec. VI.

II. SPECTRUM-EVOLUTION DYNAMICS

A. The transport equations

The evolution with range of the differential spectrum $dN_N(E,x)/dE$ is given by the integrodifferential equation (the appropriate form of the Ginzburg-Syrovatsky equation[3]):

$$\frac{\partial}{\partial x}\left[\frac{dN_N}{dE}\right]=-\int_{\bar{E}_\gamma=0}^{\infty}\sigma_{\mathrm{tot}}(E,\bar{E}_\gamma)\rho(\bar{E}_\gamma)\left[\frac{dN_N}{dE}\right]d\bar{E}_\gamma+\int_{E_0=0}^{\infty}\int_{\bar{E}_\gamma=0}^{\infty}\frac{\partial\sigma}{\partial E}(E_0,E,\bar{E}_\gamma)\rho(\bar{E}_\gamma)\left[\frac{dN_N}{dE_0}\right]d\bar{E}_\gamma dE_0\ . \quad (1)$$

Here σ_{tot} is the total cross section, or suitably isospin averaged cross section, for the process $N+\gamma\rightarrow N'+\pi$, as a function of the incident nucleon energy E_N and the photon energy and momentum. We also include other processes together with photoproduction here. It is useful to define the photon "longitudinal energy" $\bar{E}_\gamma$ by

$$\bar{E}_\gamma=\tfrac{1}{2}(E_\gamma+p_{L\gamma})=\tfrac{1}{2}E_\gamma(1+\cos\vartheta)\ , \quad (2)$$

where E_γ is the photon physical energy and where $\vartheta=0$ corresponds to the case of a "head-on" collision (photon anticollinear with the incident nucleon). The utility of Eq. (10) will be seen immediately below.

$d\sigma(E,E',E)/dE'$ is the recoil nucleon's energy distribution as a function of incident nucleon energy, photon longitudinal energy, and the recoil nucleon energy itself, E'. We shall also require the photon longitudinal energy

distribution, $\rho(\bar{E}_\gamma)$, which we obtain from the 2.7°K blackbody distribution below.

In addition to Eq. (1), we have the coupled equation describing the induced pion differential spectrum:

$$\frac{\partial}{\partial x}\left[\frac{dN_\pi}{dE}\right]=\int_E^\infty \frac{d\sigma_\pi}{dE}(E_0,E,\bar{E}_\gamma)\rho(\bar{E}_\gamma)\times\left[\frac{dN_N}{dE_0}\right]d\bar{E}_\gamma dE_0\ , \tag{3}$$

where $d\sigma_\pi(E,E',E)/dE'$ is the single-particle inclusive energy distribution of a produced pion of energy E' in terms of incident nucleon and photon energies. We can neglect the transverse momentum of the produced system with impunity in this frame (in obtaining these distributions, the transverse momentum of the produced system in the laboratory frame is, of course, relevant, but any transverse component is boosted essentially forward in this frame; we will obtain the dominant contributions from laboratory angular distributions which thus include the transverse momentum). Effectively, our present problem is one-dimensional. This equation has been used by itself to estimate the produced secondary neutrino, electron, and γ spectra assuming a fixed input spectrum $dN_N(E)/dE$. In principle, the induced neutrino spectrum is more sensitive to the original nucleon spectrum $dN_N(0,E)/dE$ than is the observed nucleon spectrum, which is essentially $dN(\langle x\rangle,E)/dE$, where $\langle x\rangle$ is the average source range. We shall neglect the produced e^+e^- pairs for which another coupled system of equations may be introduced.

Equation (1) conserves the total number of nucleons as is readily seen by noting that

$$\int_0^\infty \frac{d\sigma}{dE'}(E_0,E',\bar{E}_\gamma)dE'=\langle n_N\rangle\sigma_{\rm tot}(E_0,\bar{E}_\gamma) \tag{4}$$

and

$$\frac{\partial I_N}{\partial x}=\frac{\partial}{\partial x}\left[\int_{E=0}^\infty dE\left[\frac{dN_N}{dE}\right]\right]$$
$$=\left[-\int\sigma_{\rm tot}(E,\bar{E}_\gamma)\rho(\bar{E}_\gamma)\left[\frac{dN_N}{dE}\right]dE\,d\bar{E}_\gamma+\int dE_N\left[\frac{\partial\sigma_N}{\partial E_N}\right]\left[\frac{dN_N}{dE}\right]dE\,d\bar{E}_\gamma\right]$$
$$\propto(1-\langle n_N\rangle)\ . \tag{5}$$

As long as we are kinematically below the $N\bar{N}$ threshold we have $\langle n_N\rangle=1$, and total nucleon (plus antinucleon) number is conserved. Above threshold the total number will grow. Since the $N\bar{N}$ threshold begins at $E_N=2m_\pi{}^2/E_\gamma=3\times10^{21}$ eV and since above threshold the $N\bar{N}$ production rate is a small percentage of the total, and furthermore the incident spectrum is falling at least as fast as some (large) power of E, we may neglect $N\bar{N}$ production in the following:

Taken together, Eq. (1) and Eq. (3) conserve total energy in the absence of pair-production processes

$$E_{\rm tot}\sigma_{\rm tot}(E_0,\bar{E}_\gamma)=\int_{E_0}^\infty E\left[\frac{d\sigma_N}{dE}+\frac{d\sigma_\pi}{dE}\right]dE\ . \tag{6}$$

Furthermore, by use of Eq. (1) it is possible to understand the limits of validity of the energy loss analyses of previous authors. The total energy in the nucleon spectrum above some observable energy at a range x is

$$\mathscr{E}(E_0,x)=\int_{E_0}^\infty E\left[\frac{dN_N}{dE}(E,x)\right]dE\ . \tag{7}$$

The inelasticity of a collision is defined to be

$$\eta(E_0)=\int_0^{E_0}\left[1-\frac{E}{E_0}\right]\frac{d\sigma_N}{dE}(E_0,E)dE\left[\frac{1}{\sigma_{\rm tot}(E_0)}\right]\ . \tag{8}$$

Using Eq. (1) we may write

$$\frac{\partial\mathscr{E}(E_0,x)}{\partial x}=\int\int E\left[1-\frac{E'}{E}\right]\left[\frac{d\hat{\sigma}}{dE'}\right]\left[\frac{dN}{dE}\right]dE\,dE'$$
$$=\int E\eta(E)\hat{\sigma}_{\rm tot}(E)\left[\frac{dN}{dE}\right]dE\ , \tag{9}$$

where the caret denotes a quantity that would normally be convoluted with the 2.7°K microwave background,

$$\hat{f}(u)=\int f(u,\bar{E}_\gamma)\rho(\bar{E}_\gamma)d\bar{E}_\gamma\ .$$

Therefore, if the product $\eta(E)\sigma_{\rm tot}(E)$ is relatively slowly varying with energy, we may pull it outside the integral in Eq. (9) and arrive at the approximate energy-loss equation:

$$\frac{1}{\mathscr{E}(E_0,x)}\left[\frac{\partial\mathscr{E}(E_0,x)}{\partial x}\right]=-\hat{\eta}(E_0)\sigma_{\rm tot}(E_0) \tag{10}$$

which is the usual result. If the spectrum is falling like a power $E^{-\gamma}$ we may substitute on the right-hand side (RHS) of Eq. (10) $E\sim\mathscr{E}$, which is valid when $\gamma>1.0$. This condition must be met for the validity of previous analyses in addition to the points considered in our introduction. However, the main shortcoming of the above approximation is the fact that $\eta(E)\sigma_{\rm tot}(E)$ is certainly not a slowly varying function of energy near threshold.

B. Kinematics

The kinematics of pion photoproduction in the CRLF is straightforward. It is useful to introduce scaling variables. If $\beta=1/T$ where T is the 2.7°K photon temperature, 7.5×10^{-4} eV, then we define

$$\bar{E}_\gamma\equiv y\beta^{-1},\quad E_{N(\pi)}\equiv m_p{}^2\beta x_{n(\pi)}\ , \tag{11}$$

where $\bar{E}_\gamma$ is the photon longitudinal energy and E_N is the incident nucleon energy. The recoil nucleon has energy $E_N=z_N(m_p{}^2\beta)$. We find that $z^-\leq z_N\leq z^+$ and

$$z_n^{\pm}=x_N\left[\frac{2x_Ny+1-\mathscr{E}^2/2}{4x_Ny+1}\pm\frac{[(2x_Ny-\mathscr{E}^2/2)^2-\mathscr{E}^2]^{1/2}}{4x_Ny+1}\right], \tag{12}$$

where $\mathscr{E}=m_\pi/m_N$. Furthermore the produced pion has energy $E_\pi=z_\pi(m_\rho{}^2/\beta)$ where $z_\pi^-\le z\le z_\pi^+$ and

$$z_\pi^{\pm}=x_N\left[\frac{2x_Ny+1}{4x_Ny+1}\pm\frac{[(2x_Ny-\mathscr{E}^2/2)^2-\mathscr{E}^2]^{1/2}}{4x_Ny+1}\right]. \tag{13}$$

These kinematic limits are displayed in Fig. 1. We see in Fig. 1 that the pions will be kinematically less energetic than the recoil nucleons. At high energies the rapidity distribution of multipion production pushes most of the pions away from z_π^+ while the leading particle effect pushes the nucleon toward z_N^+.

In terms of y, the photon longitudinal-energy distribution is

$$\rho(y)=\frac{\eta}{2\pi^2}\beta^{-3}y^2\int_1^\infty\left[\exp\left[\frac{yz}{2}\right]-1\right]^{-1}z\,dz\ . \tag{14}$$

This is straightforwardly obtained from the Boltzmann distribution:

$$\rho(y)=\eta\int\frac{d^3k}{(2\pi)^3}\delta(y\beta^{-1}-\tfrac{1}{2}\,|\,k\,|\,(1+\cos\vartheta))\times\left[\frac{2}{e^{\beta|k|}-1}\right]. \tag{15}$$

Here η is an overall normalization. We numerically bin the y values and normalize the distribution numerically for the given binning, and we do not require the exact analytic value of η. We find from the above distribution that the mean value of y is ~ 3.2. Thus with $2.7\,^\circ\mathrm{K}=2.32\times10^{-13}$ GeV, the average threshold energy defined by $z_N^+=z_N^-$, is $x=0.027$, or $\sim 9.4\times10^{19}$ eV.

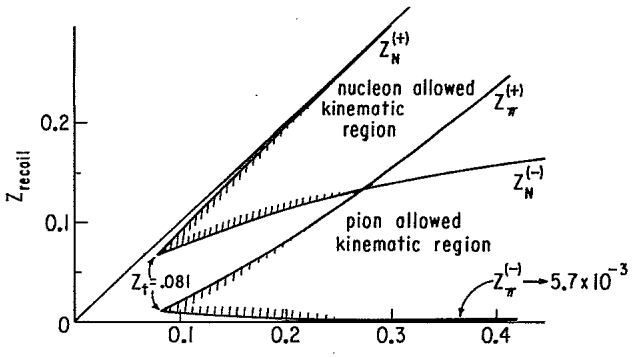

FIG. 1. Nucleon and pion kinematic regions for $y=1$ in terms of scaling variables as obtained in Eq. (22) and Eq. (23) of text. For calibration, if $T=2.7\,^\circ$K, then $z=0.1$ corresponds to 3.35×10^{20} eV and the threshold $x=0.081$ corresponds to 2.7×10^{20} eV. However, $\langle y\rangle=3.2$, and the mean threshold is 8.47×10^{19} eV, which roughly corresponds to the cutoff obtained by numerical integration.

In terms of the scaling variables the transport equations become

$$\frac{\partial}{\partial r}\left[\frac{dN_N}{dz_N}\right]=-\int\sigma_{\rm tot}(z_{N,y})\rho(y)\left[\frac{dN_N}{dz_N}\right]dy+\int\int\frac{\partial\sigma_{\rm tot}}{\partial z_N}(z_N,z'_{N,y})\rho(y)\left[\frac{dN}{dz'_N}\right]dz'_N dy\ ,$$
$$\frac{\partial}{\partial r}\left[\frac{dN_\pi}{dz_\pi}\right]=\int\int\frac{\partial\sigma_\pi}{\partial z_\pi}(z_\pi,z'_{N,y})\rho(y)\left[\frac{dN_N}{dz'_N}\right]dz'_N dy\ . \tag{16}$$

C. Photoproduction

The general features and physics of photoproductions below 3 GeV have been extensively reviewed[22] and we refer primarily to Donnachie,[22] and Genzel and Pfeil.[23] In Fig. 2 we present the total cross sections for a number of subprocesses. The gross features are similar to those of $\pi N\to N\pi$ apart from an overall normalization factor of $\sim\frac{1}{50}$. Photoproduction involves a large number of helicity and isospin degrees of freedom and entails a more involved partial wave analysis than does πN. In general, we will not be very sensitive to the rapid variations in angular distributions of produced pions or the recoil nucleon and fits to the distributions to quadratic order in $\cos(\vartheta^*)$ (ϑ^* is the c.m. production angle) will suffice. We have tested this sensitivity to higher terms and even to this order find only a 5% effect. Thus, relatively simple parametrizations and fits to the low-energy data will suffice. This is fortunate because the data is sparse in the channel $\gamma n\to\pi^0 n$.

The Δ resonance is the most conspicuous structure at $E_{\rm lab}\sim0.3$ GeV and we see that the single produced pion is the dominant component of the total cross section up to $E_{\rm lab}\sim0.8$ GeV. Above 1.0 GeV the single-pion process

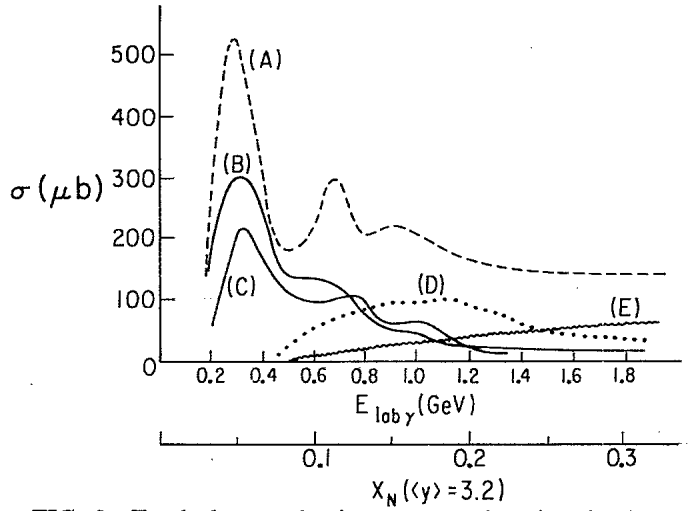

FIG. 2. Total photoproduction cross sections in microbarns vs laboratory photon energy, and x_N for $y=3.2$. (A) $\sigma_{\rm total}(\gamma p\to pX)$, (B) $\sigma(\gamma n\to\pi^- p)$, (C) $\sigma(\gamma p\to\pi^+ n)$, (D) $\sigma(\gamma p\to p\pi\pi)$, (E) upper limit to all final states with ≥3 pions on proton target. $\sigma_{\rm total}(\gamma n)$ is inferred from $\sigma(\gamma D)$ (not shown) and is to a good approximation identical to $\sigma_{\rm total}(\gamma p)$.

becomes a smaller fraction of the total cross section than the multipronged final states. The neutron and proton total cross sections are similar, the higher resonances being more conspicuous in the proton case, and both tend asymptotically to about ~ 120 mb. The neutron total cross section may be inferred from the deuteron total cross section.

Detailed angular distribution data and fits are available up to 1.5 GeV for single produced pions in all but the $\gamma n \to \pi^0 n$ reaction. The parametrizations are presented as series:

$$\frac{d\sigma}{d\Omega} = \sum_{n=1}^{N} a_n \cos^n\vartheta^* \quad (\gamma p \to \pi^0 p) ,$$

$$\frac{d\sigma}{d\Omega} = (1-\beta^* \cos\vartheta^*)^{-1/2} \sum_{n=1}^{N} a_n \cos^n\vartheta^* \quad \left[\gamma \begin{bmatrix} n \\ p \end{bmatrix} \to \pi^{\pm} \begin{bmatrix} p \\ n \end{bmatrix}\right] , \tag{17}$$

where ϑ^* (β^*) is the c.m.-system pion angle (velocity). Genzel and Pfeil[23] give tables of the coefficients a_n for various energies up to $N=6$. In Fig. 3 we present these coefficients for the process $\gamma p \to \pi^0 p$. Shown also is our fit to the coefficients for the cases of an assumed spherically symmetric distribution, and an approximation to quadratic order in the angular distribution. In practice only the spherically symmetric component is utilized because our energy-bin size causes the other components to average to zero.

In the CRLF a nucleon of incident x_N recoils into a z_N' such that $z_N^- \le z_N \le z_N^+$. We seek the recoil-nucleon z distribution which is related to the c.m. angular distribution. If we assume in the c.m. system that the incident and recoil nucleons have four-momenta given, respectively, by $P_i=(E,p,0,0)$ and $P_r'=(E',p'\cos(\vartheta^*),p_T,0)$, then we have in the CRLF

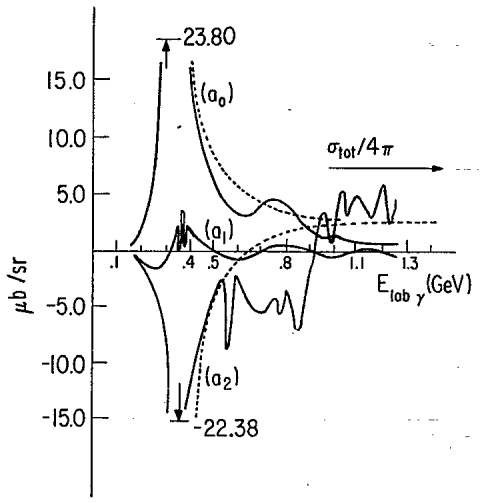

FIG. 3. Coefficients a_0, a_1, a_2 in expansion of $d\sigma/d\Omega$ for $\gamma p \to \pi^0 p$ [Eq. (26)] in μb/s vs E_{lab} taken from Genzel and Pfeil (Ref. 25). Also shown (dashed) are our fits for the spherically symmetric approximation and the test cases keeping both a_0 and a_2.

$$P_i = (\gamma(E+\beta\rho), \gamma(p+\beta E), \bar{0}_\perp) ,$$
$$P_r = (\gamma(E'+\beta\rho\cos\vartheta^*), \gamma(p'\cos\vartheta^*+\beta E'), \bar{p}_\perp) , \tag{18}$$

thus

$$z_N^{\pm} = \gamma\beta^{-1} m_p^2 (E'+\beta\rho) ,$$
$$dz_N = \gamma E' d(\cos\vartheta^*) = \tfrac{1}{2}(z_N^+ - z_N^-) d\cos\vartheta^* , \tag{19}$$
$$\cos\vartheta^* = [2z_N - (z_N^+ + z_N^-)]/(z_N^+ - z_N^-) .$$

Thus the parametrization becomes

$$\left[\frac{d\sigma}{dz_N}\right] = \sum_{n=1}^{N} a_n \left[\frac{2}{z_N^+ - z_N^-}\right] \left[\frac{2z_N - z_N^+ - z_N^-}{z_N^+ - z_N^-}\right]^n \tag{20}$$

or more conveniently

$$\frac{d\sigma_{N(\pi)}}{dz_{N(\pi)}} = \sum_{n=1}^{N} b_n^{N(\pi)} \left[\frac{z - z_{N(\pi)}^-}{z_{N(\pi)}^+ - z_{N(\pi)}^-}\right]^n \left[\frac{1}{z_{N(\pi)}^+ - z_{N(\pi)}^-}\right] , \tag{21}$$

where the b_n are now linearly related to the a_n and where N (π) denotes the nucleon (pion) case. Although this parametrization generalizes to include any degree of angular component and can incorporate the distributions of multipion final states, in practice we can safely ignore all but the $n=0$ pieces. We have verified this numerically by including $n=2$ components in rough accord with Fig. 3, and we find corrections less than 5%. The computer time savings due to neglect of these terms is of order 30%.

D. Secondary-particle production

Here we shall discuss the kinematics of the produced photons and neutrinos due to pion decay. This was previously discussed in Ref. 19, though we wish to correct a crucial typographical error in Ref. 19. In Eq. (14) of Ref. 19 there is a subscript missing; the corrected form is

$$\frac{dn_i}{dE} = \eta\theta(E_{\nu_i} - E)/E_{\nu_i} . \tag{22}$$

The photons of π^0 decay in the CRLF have energies E_1 and E_2 such that $E_1+E_2=E_\pi$ and flat distributions in energy, corresponding to spherical decay distributions in the c.m. system. The photon energies are correlated, thus for a pair we have

$$\frac{d^2N_\gamma}{dE_1 dE_2} = \int \delta(E_\pi - E_1 - E_2)\theta(E_\pi - E_1)\theta(E_\pi - E_2) \times \frac{dN_{\pi^0}}{dE_\pi} f(E_\pi) dE_\pi . \tag{23}$$

Integrating over E_π

$$N_\gamma = 2N_{\pi^0} = \int dE_\pi \left[\frac{dN_{\pi^0}}{dE_\pi}\right] E_\pi f(E_\pi) . \tag{24}$$

Thus $f(E)$ is determined and we have

$$f(E) = \frac{2}{E} , \tag{25a}$$

$$\frac{dN_\gamma}{dE}=\int\theta(E_\pi-E)\frac{2}{E_\pi}\left[\frac{dN_{\pi^0}}{dE_\pi}\right]dE_\pi\ . \tag{25b}$$

This is an essential result which we implement numerically to compute the produced photon distribution.

For the case of neutrinos from $\pi^\pm$ decay, we see that the process proceeds first through the decay $\pi\to\mu\nu$. The muon then undergoes the three-body decay, $\mu\to e\nu\nu$. Kinematically the muon in the CRLF has $E_\mu^+\geq E_\mu\geq E_\mu^-$ and satisfies

$$\frac{dN_\mu}{dE_\mu}=\tfrac{1}{2}\int\theta(E_\mu^+-E_\mu)\theta(E_\mu-E_\mu^-)(E_\mu^+-E_\mu^-)^{-1}\times\left[\frac{dN_\pi}{dE_\pi}\right]dE_\pi\ . \tag{26}$$

Neglecting the mass of the electron the three-body decay distribution satisfies

$$\frac{d^3N_{\nu_e}}{dE_1dE_2dE_3}=\int\delta(E_\mu-E_1-E_2-E_3)\theta(E_\mu-E_1)\theta(E_\mu-E_2)\theta(E_\mu-E_3)f'(E_\mu')\left[\frac{dN_\mu}{dE_\mu}\right]dE_\mu\ . \tag{27}$$

Integrating Eq. (27) we find the electron-neutrino differential distribution in terms of the muon distribution. Since the muon mass is comparable to the pion, we may approximate the muon distribution by $dN_\mu/dE\approx dN_\pi/dE$; hence,

$$\frac{dN_{\nu_e}}{dE}\cong\int E_\pi{}^{-1}dE_\pi\left[\frac{dN_\pi}{dE_\pi}\right]\ . \tag{28}$$

Hence, the electron-neutrino distribution is identical to the photon distribution to a factor of 2 in overall normalization. We will employ this approximation in our numerical analysis.

E. Numerical analysis

Our numerical-integration routine COSEV is a simple and straightforward application of the ideas discussed in this section. We bin the nucleon and pion energies, typically into 300 bins between the minimum produced pion energy, $z_\pi^{(-)}$, and a choice of upper limit, e.g., 3×10^{20} eV. We have tested the insensitivity of our results to the binning size by running tests in bin numbers ranging from 100 to 1000. We bin the photon longitudinal energies into 10 to 20 bins ranging from 0.1 $T_{2.7°K}$ to $0.4\times T_{2.7°K}$. The slowest part of the numerical procedure is in the evaluation of the integral on the RHS of Eq. (1) for each energy bin. We have found that a cubic Simpson's-rule integration routine works fine; converting to a $\log(E)$ variable is somewhat less stable numerically. Generally the effects of finite energy bin size become problematic below 100 bins, and 10 photon energy bins. Above 200 bins our precision is better than a few percent. The integration of transport equations of this kind with power-law distributions is a particularly benign problem numerically. Nonetheless, it is extremely difficult to get any useful analytical results.

We keep track of total nucleon number, interacting nucleon number, and produced pion number. By separately counting the number of interacting nucleons and the number of produced pions, which should be equal, we essentially test the precision of the nested integrations such as described above. We also keep track of the total energy. With 300 bins these quantities are controlled to 5% precision over 100 interaction lengths.

III. COSMOLOGICAL EVOLUTION

A. Source summation

We define the differential particle flux at red-shift $z=0$ for a source at distance R_0 and "activity" $\eta=\eta(E_0)=$(the integrated number of produced particles with $E\geq E_0$ per second) to be

$$j(E)=\frac{1}{4\pi R_0{}^2}\eta_0 f(E),\quad\int_{E_0}^\infty f(E)dE\equiv1\ . \tag{29}$$

The integrated flux is then

$$I(E)=\frac{1}{4\pi R_0{}^2}\int_E^\infty\eta_0 f(\tilde{E})d\tilde{E}\ . \tag{30}$$

Generally we shall assume that $f(E)$ has a cutoff E_c such that $f(E>E_c)=0$, and we shall write $f(E)=f(E_c,E)$.

The cutoff energy in the case of photoproduction and pair creation (relativistic photon targets) is determined by the photon temperature and we have $E_c\propto1/T$. A source located at red-shift z_0, cosmic coordinate r, observed at the present time, t_0, will produce a flux (we follow Weinberg,[24] Chaps. 14 and 15):

$$j(E)=\frac{\eta(z)}{4\pi R(t_0)^2r^2}f(E_c(1+z)^{-1},E(1+z))\ , \tag{31}$$

where we have introduced a z-dependent activity

$$\eta(z)=(1+z)^m\eta_0\theta(\bar{z}-z)\ ,\qquad\rho(z)=(1+z)^3\rho_0\ ; \tag{32}$$

and the evolution of the source density $\rho(z)$ is also indicated.

The activity exponent m is characteristic of "bright-phase models",[25–27] and we will find that the fits to the cosmic-ray spectrum, assuming the crossover energy is less than 10^{18} eV, will require $m\geq4$. The known activity of quasistellar objects to red-shifts of order 2, where the activity is 100× greater than at $z=0$ suggests that such an exponent is reasonable (see Schmidt in Ref. 26). Also, radio source counts suggest enhanced brightness of galaxies at smaller red-shifts.[24,27] We also see that $\eta(z)$ involves a parameter, $\bar{z}$, which is the red-shift of maximum activity. Our choice of the dependence upon this parameter is simply a guess since nothing is known about it. We will find,

however, that the induced neutrino spectrum will exhibit an energy dependence that is sensitive to $\bar{z}$ and might ultimately allow a measurement of it. We note that Hillas[7] and Blumenthal[9] have previously considered values of $\bar{z}$ as great as ~ 100.

The flux at the present epoch may be written as a volume integral in a Friedmann-Robertson-Walker metric [Weinberg[24], Eq. (15.3.3) and below]:

$$j(E)=\rho_0\eta_0 c\int_0^\infty \frac{(1+z)^{m+3}}{4\pi R(t_0)^2 r^2} f\left[\frac{E_c}{1+z}, E(1+z)\right] \times \frac{4\pi R(t_e)^3 r^2 dr}{(1-Kr^2)^{1/2}}\theta(\bar{z}-z)\ , \tag{33}$$

which upon using

$$\frac{dt}{R(t)}=\frac{dr}{(1-Kr^2)^{1/2}}\ , \qquad \frac{dz}{dt}=-(1+z)^2(1+2q_0z)^{1/2}H_0 \tag{34}$$

becomes

$$\hat{j}(E)=\frac{\rho_0\eta_0 cH^{-1}\alpha E^{-\gamma}}{(m-\gamma-\frac{1}{2})}\left\{\theta(E_c-(1+\bar{z})^2E)[(1+\bar{z})^{m-\gamma-1/2}-1] + \theta(E_c-E)\theta(E(1+\bar{z})^2-E_c)\left[\left[\frac{E_c}{E}\right]^{m/2-\gamma/2-1/4}-1\right]\right\}. \tag{38}$$

Equation (38) reveals the interesting result that for $E_c(1+z)^{-2}\le E\le E_c$, the injection spectrum index γ is modified to an observed index of $\gamma'=(m+\gamma-\frac{1}{2})/2$. For an injection index of $\gamma=2.0$ (2.5) we see that $\gamma'=3.0$ implies that $m=4.5$ (4.0). These are not unreasonable bright-phase exponents.[26,27]

The utility of Eq. (38) resides in the fact that any function may be written

$$f(E_c,E)=\int_{E_0}^\infty g(E_c,\tilde{E})\theta(\tilde{E}-E)d\tilde{E}\ , \tag{39}$$

where

$$g(E_c,E)=-\left[\frac{\partial}{\partial E}\right]f(E_c,E) \tag{40}$$

and the observed spectrum becomes

$$j(E)=\int_{E_0}^\infty g(E_c,E')\hat{j}(E',E)dE'\ . \tag{41}$$

Hence $\hat{j}(E_c,E)$ is an effective Green's function for our problem. Introducing a generalization of Eq. (46)

$$f(E_c,E)=\alpha E^{-\gamma}q(E_c,E) \tag{42}$$

and assuming that the only scales present in $q(E_c,E)$ are E_c and E, that $q(E_c,E)$ has scaling dimension zero, i.e., $q(\lambda E',\lambda E)=q(E',E)$, we obtain for Eq. (35) with $q_0=\frac{1}{2}$:

$$j(E)=\tfrac{1}{2}\rho_0\eta_0 cH^{-1}\alpha E^{-\gamma-1}\int_E^{E(1+\bar{z})^2}\left[\frac{x}{E}\right]^{1/2(m-5/2-\gamma)} \times q(E_c,x)dx\ . \tag{43}$$

$$j(E)=\rho_0\eta_0 cH_0^{-1}\int_0^{\bar{z}}\frac{(1+z)^{m-1}}{(1+2q_0z)^{1/2}} \times f(E_c(1+z)^{-1}E(1+z))dz\ . \tag{35}$$

It is useful to consider θ-function approximations to the spectrum where $\theta(x\ge 0)=1$, $\theta(x\le 0)=0$, $\partial\theta(x)/\partial x=\delta(x)$. Hence, we write

$$f(E)\equiv f(E_c,E)=\alpha E^{-\gamma}\theta(E_c-E) \tag{36}$$

and Eq. (35) becomes

$$\hat{j}(E)=\rho_0\eta_0 cH^{-1}\alpha E^{-\gamma}\int_0^{\bar{z}}\frac{(1+z)^{m-1-\gamma}}{(1+2q_0z)^{1/2}} \times\theta(E_c-(1+z)^2E)dz\ . \tag{37}$$

In flat cosmologies such as are predicted in inflationary scenarios we have $q_0=\frac{1}{2}$. Assuming this greatly simplifies our analysis and Eq. (37) becomes

This is our basic result for this section which we use for the evaluation of the cosmological component of the spectrum. A heuristic argument indicates that $q(E',E)$ will have the approximate form

$$q(E_c,E)\simeq\theta(E_c-E)+\frac{m_p}{(\gamma-1)m_\pi} \times\theta\left[E-\left[1-\frac{m_\pi}{m_p}\right]E_c\right]\theta(E_c-E) \tag{44}$$

which satisfies the scaling requirement for $q(E',E)$. Since we begin with a simple power law at injection and evolve $q(E',E)$ and we conserve baryon number, we may normalize $q(E',E)$ by

$$\int_{E_0}^\infty q(E_c,E)E^{-\gamma_i}dE\cong(\gamma_i-1)^{-1}E_0^{1-\gamma_i}\equiv\alpha^{-1}\ . \tag{45}$$

Equation (43) defines a diffuse nucleon spectrum which may fit to the observed differential spectrum for given values of z, m, and γ_i, to determine the quantity

$$\Omega_{\text{diffuse}}\equiv\rho_0\eta_0 cH^{-1}\alpha\ . \tag{46}$$

We find generally, because of the ankle and the associated anisotropy, that the assumption of an exceptionally nearby or bright source is required, e.g., the Virgo supercluster, to obtain a complete fit. From Eq. (29) with a fit including this component we obtain a result for

$$\Omega_{\text{local}}\equiv\eta_0\alpha(4\pi R_0^2)^{-1}\ . \tag{47}$$

Thus, knowing R_0 and Ω_{local} we determine $\eta_0\alpha$. Knowing

only $\Omega_{\rm local}$ and $\Omega_{\rm diffuse}$ we determine

$$\omega \equiv \Omega_{\rm diffuse}/\Omega_{\rm local} = 4\pi R_0{}^2 \rho_0 c H_0{}^{-1} = 4\pi R_0{}^2 R_{\rm IC}{}^{-3} c H_0{}^{-1} \quad (48)$$

(IC denotes "intercluster"). From this result and assuming that the cosmological sources are uniformly distributed throughout space with average separation interval at present of $R_{\rm IC}$, using $\rho_0 = 1/R_{\rm IC}{}^3$, we can deduce the ratio $R_{\rm IC}/R_0$.

B. The normalization problem

We have found the problem of the overall spectrum normalization to be sufficiently tricky that we devote the present discussion to it. We also define here a number of functions which we compute numerically and which are related to the diffuse nucleon and neutrino differential and integral fluxes through normalization factors which contain the interesting source properties.

Consider a point source at a distance R_0. We have defined the observed differential flux for the source to be

$$j(E) = \frac{\eta_0 \alpha}{4\pi R_0{}^2}\left[\frac{E_0}{E}\right]^{\gamma_i} q(E_c,E) \equiv \Omega_{\rm local}\left[\frac{E_0}{E}\right]^{\gamma_i} q(E_c,E) \quad (49)$$

in accord with the definition of $q(E_c,E)$ above. We shall take the reference energy E_0 to be 10^{18} eV in practice.

We introduce the dimensionless function

$$D(E) \equiv D(E_c,E) \equiv \frac{1}{2}\left[\frac{E_0^{\gamma_i}}{E^{\gamma_i+1}}\right]\int_E^{E(1+\bar z)^2}\left[\frac{x}{E}\right]^{1/2(m-\gamma-5/2)} \times q(E_c,x)\,d\alpha \quad (50)$$

and the diffuse cosmological component is then

$$j(E)_{\rm diffuse} = \Omega_{\rm diffuse} D(E)\ . \quad (51)$$

Typically the data is plotted in the form $(E/E_0)^3 j(E)$. We fit this to the result

$$\left[\frac{E}{E_0}\right]^3 j(E)_{\rm observed} = \left[\frac{E_0}{E}\right]^{\gamma-3} q(E_c,E)\Omega_{\rm local} + \left[\frac{E}{E_0}\right]^3 D(E)\Omega_{\rm diffuse}\ . \quad (52)$$

It is also convenient to consider the integrated flux $I(E)$. For a typical differential spectrum of the form

$$j(E) = \left[\frac{E_0}{E}\right]^{\gamma}\theta(E_c - E)\Omega_{\rm local}\ , \quad (53)$$

where $E_c \gg E_0$ we have

$$I_{\rm local}(E) = \Omega_{\rm local}\left[\frac{E_0}{\gamma-1}\right]\left[1-\left[\frac{E_0}{E_c}\right]^{\gamma-1}\right] \approx \Omega_{\rm local}\left[\frac{E_0}{\gamma-1}\right]\ . \quad (54)$$

Similarly, the diffuse spectrum may be written

$$D = \int_{E_0}^{\infty}\frac{dE}{E_0}D(E),\quad I_{\rm diffuse}(E_0) = \Omega_{\rm diffuse}E_0 D\ . \quad (55)$$

The quantity D must be computed numerically after we fold in the red-shift effects as in Eq. (37). However, for the simple θ-function spectrum of Eq. (46) we have

$$D(E) = \frac{1}{(m-\gamma-1}\left\{\theta(E_c - E(1+\bar z)^2)[(1+\bar z)^{m-\gamma-1/2}-1] + \theta(E(1+\bar z)^2 - E_c)\theta(E_c-E)\left[\left[\frac{E_c}{E}\right]^{m/2-\gamma/2-1/4}-1\right]\right\} \quad (56)$$

and, assuming $E_0(1+\bar z)^2 > E_c$ (or $\bar z \gtrsim 9$) we find

$$D = \left[\frac{1}{2p}\right]\left[1+(p-1)^{-1}\left[\frac{E_c}{E}\right]^p - p(p-1)^{-1}\left[\frac{E_c}{E}\right]\right], \quad (57)$$

where $p = m/2 - \gamma/2 - \frac{1}{4}$ and typically $\gamma = 2.5$, $m = 4.0$, so $p = \frac{1}{2}$. Therefore,

$$I(E_0)_{\rm observed} = \Omega_{\rm local}\left[\frac{E_0}{\gamma-1}\right]\left[1-\left[\frac{E_0}{E}\right]^{\gamma-1}\right] + \left[\frac{1}{2p}\right]\Omega_{\rm diffuse}\left[1+(p-1)^{-1}\left[\frac{E_c}{E}\right]^p - p(p-1)^{-1}\left[\frac{E_c}{E}\right]\right] \quad (58)$$

(here γ is the injection slope, not the observed slope).

In general we will distinguish between the cutoff in the local component and the cutoff in the diffuse component. This is due to the fact that the effects of pair creation have little impact upon the local contribution, but will significantly reduce the cutoff in the diffuse component.

For the ν_e spectrum we first note that we can directly compute the ratio of induced ν_e's to nucleons at range R_0:

$$I_{\nu_e}(E \geq 0)/I_N(E_0) \equiv c(\gamma_i, E_0) f(R_0) \quad (59)$$

by numerical integration of the spectrum evolution transport equations. Here $f(R_0)$ is the fractional yield of neutrinos produced at range R_0 and $f(\infty) = 1$. We derive

$c(\gamma_i,E)$ and f numerically and give results in Table I. We define the ν_e spectrum induced from a point source of nucleons at range R_0 to be

$$j_{\nu_e}(E)=\frac{\eta_0\epsilon f(R_0)}{4\pi {R_0}^2}S(E_c,E)=\Omega_{\text{local}}f\epsilon S(E_c,E)\ , \tag{60}$$

where $S(E_c,E)$ is the function of Fig. 8(b) with the normalization $S(E_0,E_0)=1.0$. This function is weakly dependent upon the injection index of the nucleon spectrum, unless one is interested in the highest-energy neutrinos, $>10^{19}$ eV. The properties of this function are derived numerically in the next section, but we note that Fig. 9 displays the departure from universality of the high-energy end of the neutrino spectrum for different injection indices.

The integrated ν_e flux is then

$$\begin{aligned}&\int_0^\infty j_{\nu_e}(E)dE=\Omega_{\text{local}}f\epsilon T(E_c)\ ,\\ &T(E_c)=\int_0^\infty S(E_c,E)dE,\quad T(E_c)\equiv E_0T\ ,\end{aligned} \tag{61}$$

and the numerical result for the normalization constant T is found to be $T=10.67$. Hence

$$\begin{aligned}I_{\nu_e}(0)_{\text{local}}/I_N(E_0)_{\text{local}}&=f\epsilon(\gamma-1)T\\ &=fc(\gamma_i,E_0)\ ,\\ \epsilon&=c(\gamma_i,E_0)/[(\gamma-1)T]\ .\end{aligned} \tag{62}$$

Thus the local differential spectrum is

$$j_{\nu_e}(E)=\Omega_{\text{local}}c(\gamma_i,E_0)S(E_c,E)f(R_0)/[(\gamma-1)T]\ . \tag{63}$$

The diffuse cosmological ν_e spectrum may be obtained with the aid of Eq. (43). Note first that $\gamma=0$. Second, the differential ν_e spectrum produced at red-shift $1+z$, observed at $z=0$ will take the form

$$j_{\nu_e}(E,z)=\frac{\eta(z)}{4\pi R^2(0)r^2}(1+z)^{\gamma+1}S[E_c,E(1+z)^2]\epsilon \qquad [f\approx f(\infty)=1]\ . \tag{64}$$

This is due to the fact that it is $I_{\nu_e}(0)/I_N[E_0/(1+z)]$ that remains constant and thus the produced ν_e's will be in a greater abundance by a factor of $(1+z)^{\gamma-1}$ at red-shift z, following the increased integrated number of active nucleons as the threshold is reduced. But, the reduction in threshold gives an effective reduction in T by a factor of $1/(1+z)^2$ [we integrate in Eq. (61) up to an upper limit of $E_c/(1+z)^2$; this is the effective increase in the normalization of the function $S(E_c,E)$ as E_c is reduced to $E_c/(1+z)^2$].

Again, it is useful to introduce a dimensionless function, $G(E_c,E)=G(E)$, by

$$G(E)=\tfrac{1}{2}\int_E^{E(1+\bar{z})^2}\left[\frac{x}{E}\right]^{(1/2)(m-3/2+\gamma_i)}S(E_i,x)\frac{dx}{E} \tag{65}$$

and the normalization constant is defined

$$G=\int_{E_0}^\infty G(E_c,E')\frac{dE'}{E_0}\ . \tag{66}$$

Therefore, the cosmologically evolved neutrino differential spectrum becomes

$$j_{\nu_e}(E)_{\text{diffuse}}=c(\gamma_i,E_0)\Omega_{\text{diffuse}}G(E)/[(\gamma_i-1)T]\ , \tag{67}$$

where $\gamma_i=\gamma_{\text{injection}}$.

Remarkably we see in Eq. (65) that the bright-phase parameter m and the injection nucleon index γ_i enter in the combination $m+\gamma_i$. This is related directly to the observed cosmic-ray spectrum slope by $\gamma_{\text{observed}}=(m+\gamma_i-\frac{1}{2})/2$. Hence, the neutrino spectrum only depends upon the observed nucleon index, and we see in Eq. (65) that to a very good approximation the slope of the produced diffusion neutrino spectrum will be $\gamma_0+(\frac{1}{2})$. We may write for the integrated diffuse ν_e component above the reference energy E_0:

$$I_{\nu_e}(E_0)=E_0G\epsilon\Omega_{\text{diffuse}}=\frac{c(\gamma_i,E_0)GI_{N\text{diff}}(E_0)}{2(\gamma_i-1)TD}\ . \tag{68}$$

The parameters defined presently are numerically evaluated in the following section. The forms derived by θ-function approximations are generally sufficiently accurate for analytic estimates.

IV. NUMERICAL RESULTS

In Figs. 4–6 we present the results of evolving injection spectra with indices $\gamma_i=3.0$ through 2.0 using the full transport evolution equations while neglecting cosmologi-

TABLE I. The "kinematic" quantities pertaining to a given injection slope γ_i. We give (i) D, the normalization of $D(E)$ above 10^{18} eV computed numerically; (ii) $c(\gamma_i,10^{18}\text{ eV})$, the neutrino yield at infinite range; (iii) $\epsilon(\gamma_i)$, the "differential neutrino yield" defined in Eq. (61); (iv) f, the fraction of neutrinos produced by 3 IL to those produced at infinity; (v) the requisite bright-phase index to fit the observed $\gamma_{\text{obs}}=3.0$ for $q_0=\frac{1}{2}$ for given γ_i.

γ_i	D	$c(\gamma_i,10^{18}\text{ eV})$	$\epsilon(\gamma_i)$	f(3 IL)	m
3.0	1.00	2.48×10^{-4}	1.16×10^{-5}	0.370	3.5
2.5	1.20	2.17×10^{-3}	1.36×10^{-4}	0.399	4.0
2.2	2.20	7.85×10^{-3}	6.13×10^{-4}	0.420	4.3
2.0	3.42	1.85×10^{-2}	1.73×10^{-3}	0.431	4.5
1.8	5.45	3.86×10^{-2}	4.52×10^{-3}	0.468	4.7
1.5	11.46	1.17×10^{-1}	2.19×10^{-2}	0.531	5.0

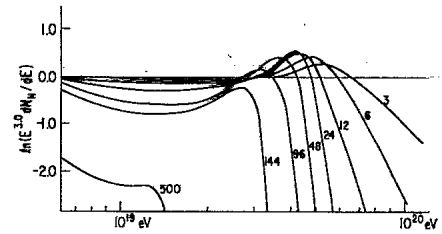

FIG. 4. Evolved $1/E^{3.0}$ injection spectrum to 500 interaction lengths. 1 IL=6 Mpc. Injection spectrum is normalized to unity at 10^{18} eV. This may be taken as a good approximation to $q(E_c,E)$ for $\gamma_i=2.0$.

cal effects. 1 IL (interaction length) corresponds roughly to 6 Mpc and 500 IL roughly corresponds to R_H, the Hubble length scale. Thus, the neglect of red-shift effects in these figures makes them inapplicable as final results beyond 100 Mpc or about 12 to 24 IL. However, these are suitable results for nearby sources and as inputs to the formulas of Sec. III for the computation of red-shift effects. All of these results were obtained with the spherically symmetric angular distribution assumption for photomeson production, and with Blumenthal's results for pair creation.[9]

Figure 4 contains an evolved $1/E^{3.0}$ injection spectrum. To a good approximation this is equivalent to the result for $q(E_c,E)$ for injection spectra with slopes as flat as 2.0. We assume an artificial numerical cutoff of 3×10^{20} eV (at most a 10% normalization correction above 10^{20} eV). After 3 IL the appearance of the cutoff and the pile-up are seen. The pile-up peak reaches a maximum at a range

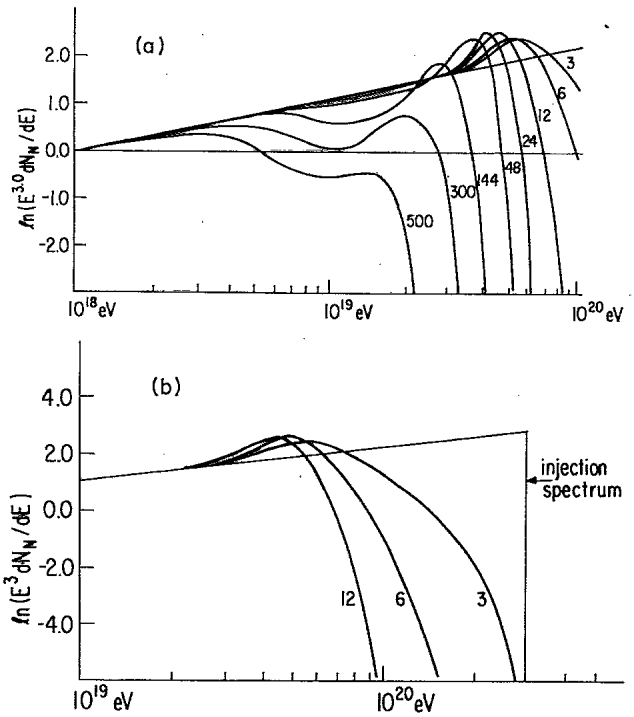

FIG. 5. (A) Evolved $1/E^{2.5}$ injection spectrum normalized to unity at 10^{18} eV. 1 IL=6 Mpc. The dip structure and the downward evolution of the pile-up with increasing range are clearly seen. (B) High-energy behavior of $1/E^{2.5}$ injection spectrum. Note that injection spectrum is cut off at 3×10^{20} eV.

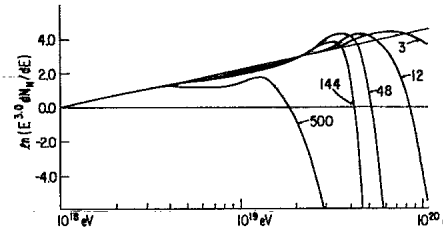

FIG. 6. Evolved $1/E^{2.0}$ injection spectrum normalized to unity at 10^{18} eV. 1 IL=6 Mpc.

of order 24 IL. Here it is about $1.6\times$ the flat injection spectrum lying in the range 3.0 to 5.0×10^{19} eV. Beyond this range the effects of pair creation become pronounced. We see the gradual shifting of the pile-up toward lower energies and the new feature: the appearance of a "dip" onsets at 0.7 to 2.0×10^{19} eV. The dip occurs because here we have the peaking of the pair-creation energy-loss effect (see Blumenthal, Ref. 9, Fig. 4) while the large "pile-up" remains above this energy scale. The result is much like that of a snake digesting a small pig, and the pile-up slowly moves to lower energies while the spectrum is significantly reduced at slightly lower energies. The pile-up is not easily "digested" and remains quite conspicuous out to even 500 IL. By 144 IL the pile-up drops below the normalization of the input spectrum.

In Fig. 5(a) we present the evolution of the $1/E^{2.5}$ injection spectrum. The function of $q(E_c,E)$ can be inferred by subtracting the injection spectrum from the plotted spectrum in the logarithmic plot. In Fig. 5(b) we present the high-energy end of the spectrum which shows our artificial numerical cutoff on the injection spectrum. Unfortunately, we become increasingly sensitive to this cutoff as the injection slope is reduced, and we have not carried out runs with a numerical cutoff much larger than 3×10^{20} eV. Thus, our results above 10^{20} eV should not be taken too seriously, and for $1/E^2$ injection slope they are expected to have 30% corrections.

In Fig. 6 we present the $1/E^{2.0}$ injection slope results, and our ordinate scale is changed to accommodate the results. Thus, the dip and pile-up are less conspicuous here but do occur with approximately universal structure after 100 IL. We have not run $1/E^{1.5}$ injection spectra, or flatter, but may infer the general behavior of such from the $1/E^{2.0}$ results.

In Fig. 7 we present the evolution of the number of produced secondary electron neutrinos with range for each of the injection spectra. The injection spectra are each normalized to unity at 10^{18} eV thus the asymptotic values plotted in Fig. 7 represent the quantity $c(\gamma_i,10^{18}\text{ eV})$ defined in Sec. III. Obviously the neutrino yield increases with the flattening of the injection spectrum and closely follows the integrated number of nucleons above 10^{20} eV in the injection spectrum, i.e., we see that the neutrino yields are in the ratio 1:10:100 for injection indices 3.0:2.5:2.0. We have previously run simulations without the effects of pair creation and found that many more secondary neutrinos were produced and that the approach to asymptopia is much slower. The pair-creation effects, by reducing the pile-up to lower energies, accelerates this approach, and thus simplifies our problem of including

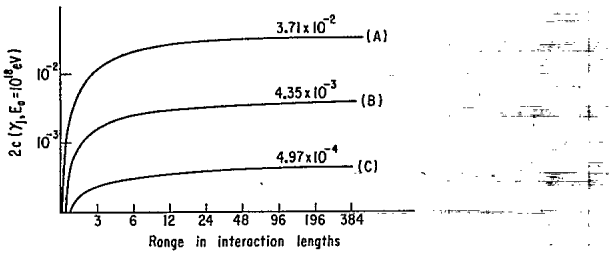

FIG. 7. Neutrino yield with range for (A) $1/E^{2.0}$; (B) $1/E^{2.5}$, (C) $1/E^{3.0}$ injection spectra. This is the function $2[c(\gamma_i,E_0)=I_{\nu_e}(0)/I_N(10^{18})]$. The numbers refer to the asymptotic yields used in normalizing the cosmological neutrino spectrum. The approach to asymptopia is slower without the pair-production effects and higher neutrino yields would occur.

the red-shift and cosmological-source sums.

In Fig. 8(a) we present the successive pile-up of produced pions with an arbitrary normalization (which we do not require, but which must be consistent with the normalization of Fig. 7 for the integrated spectra). In Fig. 8(b) we give the neutrino spectrum with range, or equivalently the function $S(E_c,E)$ defined in Sec. III, which is normalized to unity at $E=0$. The resulting $S(E_c,E)$ is essentially independent of the injection slope for energies less than 10^{19} eV.

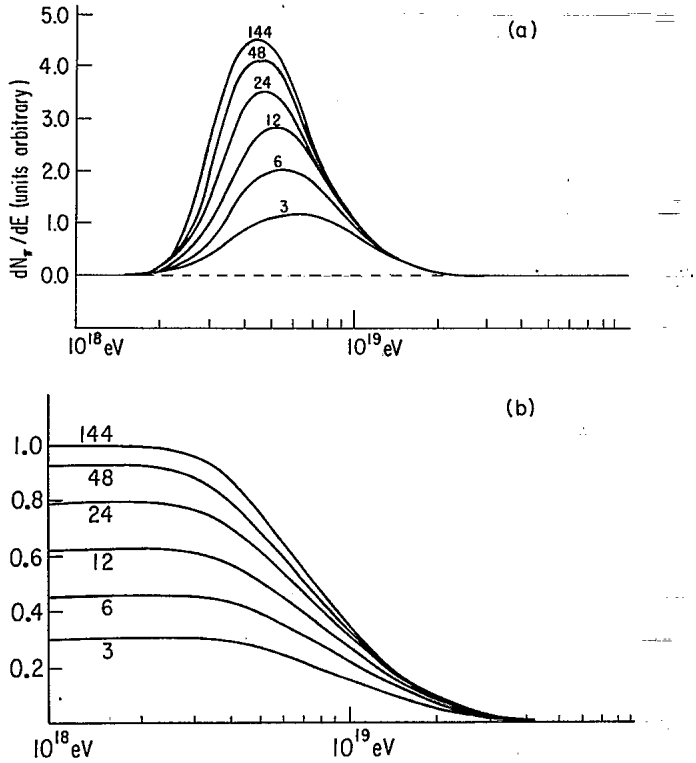

FIG. 8. (A) The evolution of the differential pion distribution from which we derive the differential neutrino (and photon) distributions. We establish the normalizations of these latter distributions separately, and the pion distributions here have arbitrary normalization. (B) Evolution of the neutrino differential spectrum with range normalized to unity at $E\to 0$. This is the function $S(E_c,E)$ defined in Sec. III used in computing the cosmological flux. This plot is for the case of a $1/E^{2.5}$ injection spectrum, but the result is universal below 10^{19} eV.

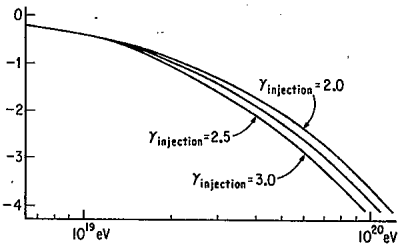

FIG. 9. Departure from universality in $S(E_c,E)$ at high energy is seen here for different input spectra. Since fluxes are so low at these energies, we neglect these effects.

However, there are departures from universality for various injection spectra in $S(E_c,E)$ above 10^{19} eV as is seen in Fig. 9. Obviously, the flatter injection spectra produce a more copious yield of UHE neutrinos. However, if one measures the slope of $S(E_c,E)$ above 10^{19} eV one finds a rapid cutoff of $\sim 1/E^{4.0}$. This is essentially the effect of the kinematics of the produced pion as seen in Fig. 1 and in the produced pion distributions of Fig. 8(a), and thus the search for electron neutrinos above 10^{19} eV produced by this mechanism would not be too promising. Since it is difficult to imagine any other mechanism for producing UHE neutrinos (they are uncharged and do not participate in dynamo effects; other collision processes are unlikely as per Sec. III). The interesting range to study would appear to be 10^{18} eV up to 10^{19} eV.

Since a universal differential neutrino spectrum is produced after a few tens of interaction lengths by any given source with a normalization that is simply related to the injection slope, it becomes a simple matter to compute the cosmological neutrino flux of unit normalization, i.e., we present the function $G(E_c,E)=G(E)$ in Fig. 10 as defined in Sec. III. In using this result to predict an observable neutrino flux, we first determine the coefficient $\Omega_{\rm diff}$ of the cosmological nucleon-flux component and write

$$j_{\nu_e}(E)_{\rm diffuse}=\Omega_{\rm diff}\frac{c(\gamma_i,E_0)G(E)}{(\gamma_i-1)T}$$
$$=I_{N\rm diff}(E_0)\frac{c(\gamma_i,E_0)G(E)}{(\gamma_i-1)TDE_0} \qquad (69)$$

for injection index γ_i. The quantity $c(\gamma_i,10^{18}\text{ eV})$ is tabulated in Table I for various injection indices and $T=10.67$ is the normalization of $S(E_c,E)$ divided by 10^{18} eV. D is the normalization of the diffuse component spectrum, $D(E)$ and is also given in Table I. Thus, for example, if the observed integrated spectrum above 10^{18} eV is $I_N(10^{18}\text{ eV})=I_{\rm diff}(10^{18}\text{ eV})=I_0$, and if we take an injection index $=2.5$, then we find that $c(2.5,10^{18}\text{ eV})=2.17\times10^{-3}$, and $D(2.4)=1.20$, we obtain

$$j_{\nu_e}(E)=I_N(10^{18}\text{ eV})[1.1\times10^{-5}G(E)\times10^{-18}\text{ eV}^{-1}]\,. \qquad (70)$$

As described in Sec. III, to a good approximation $G(E)$ falls like $1/E^{3.5}$ above the energy scale 5×10^{18} eV$/(1+\bar{z})^2$. Below this scale the spectrum must flatten, and its observation can in principle reveal the quantity $\bar{z}$. The actual high-energy behavior of $G(E)$ is presented in

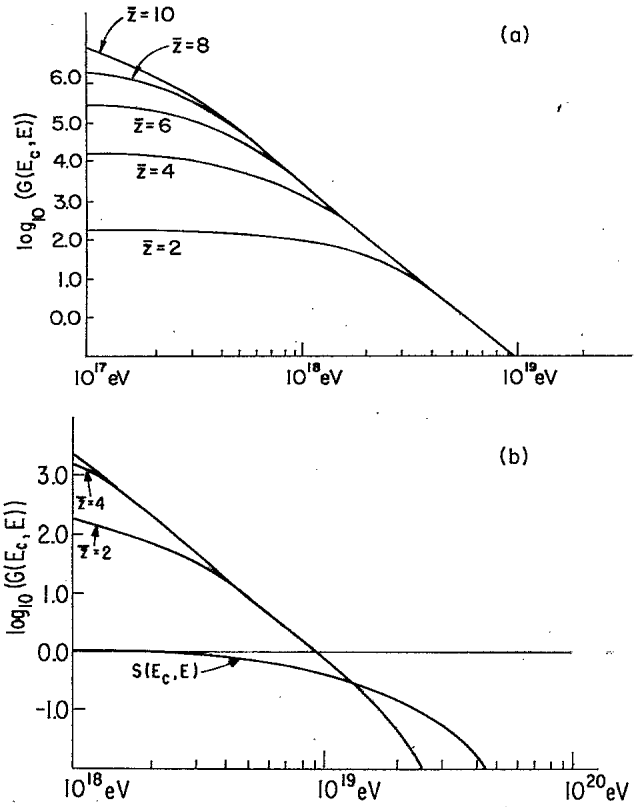

FIG. 10. (A) The cosmological neutrino spectrum with "unit normalization," i.e., this is the function $G(E_c,E)$ defined in Sec. III, evaluated for different maximum-brightness red-shifts $\bar{z}$. The curves become universal at high energies. In principle, the observation of the rollover would constitute a measurement of $\bar{z}$. $q_0=\frac{1}{2}$ is assumed. The high-energy slope is $\gamma_{\text{observed}}+\frac{1}{2}$, independent of m and $\gamma_{\text{injection}}$. (B) High-energy behavior of $G(E_c,E)$ and $S(E_c,E)$ for comparison. We assume a universal $S(E_c,E)$ for the evaluation (we use $\gamma_i=2.5$ as in Fig. 9).

Fig. 10(b) and we readily see that above 2×10^{19} eV the spectrum steepens and drops much faster than $1/E^{3.5}$. Our numerical evolution is insensitive above this scale.

The integrated neutrino spectrum is given by

$$I_{\nu_e}(10^{18}\text{ eV})=\frac{\Omega_{\text{diff}}I_N(10^{18}\text{ eV})Gc(\gamma_i,10^{18}\text{ eV})}{(\gamma_i-1)TD} \tag{71}$$

and we thus obtain for the example above $I_{\nu_e}(10^{18}\text{ eV})=1.06\times10^{-1}I_0$. The integrated flux falls roughly as $1/E^{2.5}$.

In computing the cosmologically evolved nucleon spectrum we encounter an ambiguity. Our assumption in Sec. III was that the nucleon spectrum would undergo a rapid evolution due to photomeson production and then become stable. In that case, we would insert the stable fully evolved spectrum, $q(E_c,E)$, into Eq. (60) for the function $D(E)$ and obtain an unambiguous prediction for the diffuse spectrum. However, as Figs. 4–6 reveal the spectrum is far from stable after 20 IL due to the effects of pair creation and the gradual shift of the pile-up to lower energies. Thus the dilemma arises in the present approximation which spectra at which range should be used as the input to Eq. (59)?

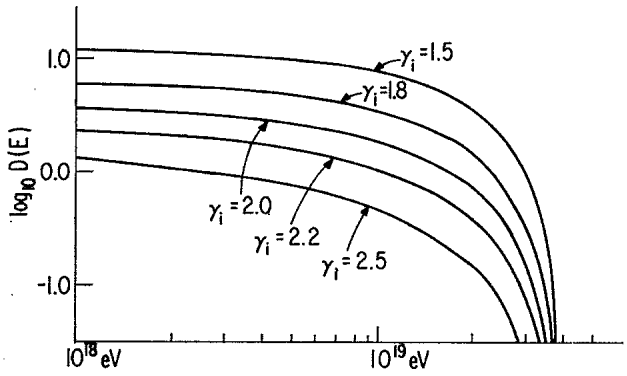

FIG. 11. The diffuse nucleon spectrum of normalization D as defined in Sec. III. The true cutoff is less well defined than the cutoff here of order 4×10^{19} eV based upon a 144-IL input for $q(E_c,E)$ for $\gamma_i=2.0$.

A sum over distant sources either weights the nearest or the most distant sources preferentially. In the present case of a bright phase index $m=4$ to 5 we preferentially weight the most distant sources. Therefore, we might use the 500-IL spectrum as input since the 24-IL spectrum would lead to an overestimate of the effective cutoff energy. However, by doing this we somewhat underestimate the spectrum above 2×10^{19} eV. This has the effect of overemphasizing the dip structure seen in the data. We have opted instead to use the approximate geometric mean of the two extremes, 144 IL as our input for $q(E_c,E)$. We have found that this does not qualitatively change the results, though the dip is least conspicuous with the 24-IL input. A better computation would input a "moving" $q(E)$ with z, but then sacrifice the simplicity of Eq. (50).

In Fig. 11 therefore we present the result of the cosmological convolution integral, i.e., the function $D(E)$ defined in Sec. III for the various injection spectra γ_i. Actually, we have made an additional approximation here which is to use the 144-IL function $q(E_c,E)$ derived from the $\gamma_i=2.0$ case for each injection spectrum. In actuality the cutoff should not be so abrupt at 2×10^{19} eV, and it should not be exactly the same for each injection spectrum. However, these departures from universality should not be much more severe than those seen in the preceding examples. We find in Sec. IV that the $1/E^{2.0}$ fit is the best.

The normalization of the $D(E)$ is given as the quantity D for energies above 10^{18} eV and clearly differs among the spectra.

IV. A MODEL OF THE ULTRAHIGH-ENERGY SPECTRUM

Armed with the analyses of Secs. II and III we are ready to attempt a model fit to the ultrahigh-energy-nucleon spectrum and to make predictions for the neutrino spectrum. Unfortunately we will be limited by the available data, but our approach is sufficiently general that it may be updated as more data accrues.

Throughout we will fit exclusively to the Haverah Park data as presented by Cunningham *et al.*[14a] and Brooke *et al.*[14b] This is a matter of convenience; the Haverah

Park data is the largest single and thus internally consistent set and we need not worry about relative calibration errors between different facilities. Nonetheless, we do not do justice to the existing data presently because we have not developed a detailed understanding of the experimental errors. We have inferred the error from a careful scrutiny of the figures in the principal references and comparisons of reported estimates against our own. We feel a more complete error analysis would be of considerable use. Also, it is difficult to interpret the statistical variables when the errors are increasing monotonically with the energy; a χ^2 measurement above 10^{18} eV is virtually insensitive to the ankle, while the relative normalizations of energy bins in the ankle are statistically significant.

The idea presently is not new but the methods based upon the earlier discussions in this paper are. Thus the results are entirely new and supersede most previous analyses involving the GZ cutoff and induced neutrinos. We shall assume that the UHE cosmic-ray spectrum is of a cosmological origin and composed of two components: (1) A diffuse cosmological component of strength $\Omega_{\rm diff}D(E)$ which has been steepened from an injection index γ_i to an observed $\gamma_{\rm obs}=3.0$ by the cosmological red-shift effects and the bright-phase activity discussed in Sec. III. This is the idea of Hillas[7] and implemented with pair production by Blumenthal.[9] (2) A semilocal component which we write as $\Omega_{\rm Virgo}q(E)/E^{\gamma_i}$, which we identify with the Virgo cluster as containing a source or sources at a range ~ 3 IL with respect to photomeson production. This idea has been employed previously by Wolfendale and collaborators in Ref. 8. One might further postulate a local component primarily composed of Fe originating within our galaxy and subject to the effects of local steering. Our assumption presently will be that the crossover energy occurs at a scale small relative to 10^{18} eV and that only the cosmological and semilocal components appear at this energy. This is, of course, related to the red-shift of maximum activity and for $E_{\rm crossover}<10^{18}$ eV we require $\bar{z}>10$.

Why should we superimpose the diffuse component and the semilocal component? We find in our fits that the normalization of the diffuse component will imply an average source separation of order 100 Mpc. This is, remarkably, the scale of supercluster hierarchies. Of course, the Virgo cluster is only 20 Mpc in range and should be ~ 25 times brighter than the first diffuse components. The diffuse component will cutoff at a scale of order 4×10^{19} eV since it will be dominated by the effects of the most distant sources (there will be a correction of order 20% to this by our neglect of the nearest sources in the source sum integral, i.e., the nearer diffuse components do not cutoff until about 6×10^{19} eV), while the semilocal component will be enhanced at 8×10^{19} eV by the pile-up and the flatter injection index. Both the diffuse and semilocal components will produce neutrinos, and an anisotropy will occur in the highest energies associated with the direction of Virgo.

It is conceivable that the crossover is just occurring at a scale of $\sim 10^{19}$ eV in which case a three-component model is required. Here we assume that the Virgo cluster is responsible for the anisotropy and is emerging as the ankle structure in the spectrum as well. But, we may then turn the argument around and assume a supercluster interspacing of order 100 Mpc for clusters of similar activity to Virgo to obtain an estimate of $\Omega_{\rm diff}$, and then to obtain a prediction for the neutrino spectrum, even though the diffuse contribution to the nucleon spectrum is masked by a local component. The result of this exercise will be similar to the results obtained here.

In Fig. 12 we present the Haverah Park data, excluding the most recent events reported at the 18th International Cosmic Ray Conference.[16] To this data we fit the composite spectrum

$$j_N(E)=\Omega_{\rm diff}D_{\gamma_i}(E)+\Omega_{\rm Virgo}j_{\rm local}(E)\ , \tag{72}$$

where $D(E)$ is the evolved diffuse spectrum function of Fig. 11 and $j_{\rm local}(E)$ is the 3-IL evolved injection spectrum normalized to unity in Figs. 4–6. For tests with spectra flatter than 2.0 we assume the $q(E_c,E)$ obtained for the $\gamma_i=2.0$ case.

In Fig. 12 we also show the results of our three best fits to this data. These correspond to $\gamma_i=2.2$, $\gamma_i=2.0$, and $\gamma_i=1.8$, respectively, yielding $\chi^2=2.94$, 2.14, and 2.67. The best fit with $\gamma_i=3.0$ has $\chi^2=2.95$ and results in $\Omega_{\rm diff}=0.0$. The χ^2 reported here is for all bins above 10^{18} eV, while for those bins above 5×10^{18} eV we obtain $\chi^2=(2.72,1.90,1.69)$, respectively. In Table II we present the results for the parameters of these fits.

In addition to the ankle, a striking result here is the appearance of the dip structure at the scale $\sim 10^{19}$ eV. This structure is visually present and appears to be statistically significant. One can find the best straight-line fit to the data above 10^{18} eV which has χ^2 of 3.54, and corresponds to an ordinate of 1.06 in Fig. 12. Above 5×10^{18} eV the same straight-line fit has a χ^2 of 3.07, while the best line now has $\chi^2=2.38$ and an ordinate value of 0.95. With the existing statistics, these measures are not very meaningful and we await the accrual of more data.

The dip must always arise in our model because of the "minicrossover" from the diffuse component of the semilocal one at about 10^{19} eV. However, as we mentioned in Sec. III, the ambiguity in the choice of an input $q(E_c,E)$

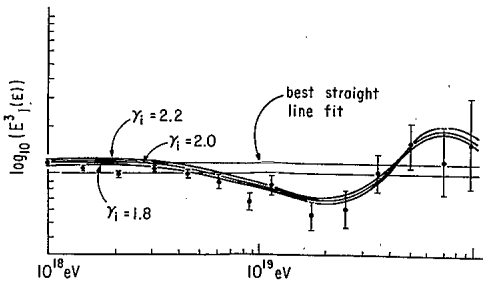

FIG. 12. The Haverah Park data (not including the most recently reported events of the 18th International Cosmic Ray Conference and dropping the least statistically significant bins at 1.3×10^{20} eV and 2×10^{20} eV corresponding to $\log_{10}[E_0{}^3(E)]=0.13\pm0.5$ and 0.47 ± 0.6, respectively). Also shown are our three best fits. The dip is seen and our fit accommodates the ankle structure (with the exception of these highest bins).

TABLE II. The results of two-component-model fits to the Haverah Park spectrum data. (i) $\Omega_{\rm diff}$ is the coefficient of the diffuse component of the differential spectrum in units of $I_N(10^{18}\ {\rm eV})/(10^{18}\ {\rm eV})\equiv J$. (ii) Ω_V is the semilocal coefficient in units of J. (J so defined is, using Haverah Park data, $2.53\pm0.08\times10^{-34}/{\rm cm^2 s\ sr}$.) (iii) $\omega=\Omega_{\rm diff}/\Omega_V$. (iv) $R_{\rm IC}$ is the effective diffuse-source separation in (Mpc)$h_0^{-1/3}$ as obtained from the fit. (v) χ_E^2 is for the given fit including data above E (in GeV). (vi) $I_{\nu_e}(E)$ is the integrated neutrino yield above E for the fit.

γ_i	$\Omega_{\rm diff}$	Ω_V	ω	$R_{\rm IC}$	$\chi^2_{10^{18}}$	$\chi^2_{5\times10^{18}}$	$I_{\nu_e}(10^{18})$	$I_{\nu_e}(10^{19})$
2.5	0.70	0.241	2.9	1.73×10^2	10.62	10.44	0.125	3.9×10^{-4}
2.2	0.43	7.15×10^{-2}	5.98	1.36×10^2	2.94	2.72	0.344	1.09×10^{-3}
2.0	0.29	2.04×10^{-2}	14.04	1.02×10^2	2.15	1.90	0.652	2.06×10^{-3}
1.8	0.18	1.22×10^{-2}	14.9	1.00×10^2	2.68	1.71	1.07	3.38×10^{-3}
1.5	8.69×10^{-2}	4.04×10^{-3}	21.5	0.88×10^2	8.44	7.35	2.50	7.91×10^{-3}

in the evaluation of $D(E)$ slightly exaggerates the dip. We believe that the dip may ultimately be a reliable feature in the spectrum compelling this kind of a model. We note that in the spectrum figure of Cunningham *et al.*[16a] the dip is visually present in all other order data sets of other groups, and we encourage experimentalists to give it an unbiased study. We warn the reader that the dip (or even the ankle) may be a phenomenon associated with a rapid phase change in the anisotropy and the detector response to such. Thus, further experimental analysis of the hypothetical dip structure is needed.

We see that our fits give an ankle structure in qualitative agreement with the reported data, though statistically this result is not yet very meaningful.

We obtain directly from our fits the ratio

$$\omega=\Omega_{\rm diffuse}/\Omega_{\rm local}=4\pi R_{\rm Virgo}{}^2\rho_0 cH_0{}^{-1}\ , \tag{73}$$

where $R_{\rm Virgo}$ is the range of Virgo, 20 Mpc, and the Hubble length is $cH_0{}^{-1}=h_0{}^{-1}(3\times10^2)$ Mpc, and ρ_0 is the supercluster density $\sim 1/R_{\rm IC}{}^3$ where $R_{\rm IC}$ is the intercluster spacing. We find therefore

$$R_{\rm IC}=h_0{}^{-1/3}\omega^{-1/3}(2.47\times10^2\ {\rm Mpc})\ . \tag{74}$$

The natural expectation the $R_{\rm IC}\sim100$ Mpc emerges from our fits. Also, we have from the integrated normalizations of $j_{\gamma_i}(E)$ and the $D(E)$ the result for the integrated flux above 10^{18} eV:

$$I_N(10^{18}\ {\rm eV})/10^{18}\ {\rm eV}=(\gamma_i-1)^{-1}\Omega_{\rm Virgo}+D_{\gamma_i}\Omega_{\rm diffuse}$$
$$=\Omega_{\rm Virgo}[(\gamma_i-1)^{-1}+D\omega)]\ , \tag{75}$$

where D is given in Table I. These parameters are given in Table II.

From these results we obtain crude anisotropy estimates. In Fig. 13 we plot

$$a\equiv\frac{\Omega_{\rm Virgo}j_{\gamma_i}(E)}{\Omega_{\rm diffuse}D(E)+\Omega_{\rm Virgo}j_{\gamma_i}(E)} \tag{76}$$

for our three best fits. This assumes that pure Virgo cluster yields an anisotropy of 100% and pure diffuse yields 0% (a residual galactic contribution might show up here at low energies). We plot also the anisotropy data of Ref. 16. Remarkably, our best spectrum fit appears to be in best agreement with the anisotropy as well, though we have not carried out a statistical comparison. It is interesting that the χ^2 minimum is closest to the reported anisotropy.

From the values of the parameters derived by the best fit to the spectrum, we can obtain predictions for the resulting electron-neutrino spectrum and anisotropy. We have

$$j_{\nu_e}(E)=\Omega_{\rm Virgo}\epsilon S(E)+\Omega_{\rm diffuse}\epsilon G(E) \tag{77}$$

and the anisotropy

$$a_{\nu_e}(E)=\frac{\Omega_{\rm Virgo}S(E)}{\Omega_{\rm diffuse}G(E)+\Omega_{\rm Virgo}S(E)}\ . \tag{78}$$

These are plotted in Fig. 14.

The integrated flux of neutrinos above 10^{18} eV is then

$$I_{\nu_e}(10^{18}\ {\rm eV})=(10^{18}\ {\rm eV})\Omega_{\rm Virgo}[c(\gamma_i,E_0)+\omega G\epsilon]\ , \tag{79}$$

where the parameters are given in Table I.

The best fit to the spectrum with $\gamma_i=3.0$ excludes the diffuse component altogether. Nonetheless, for injection spectra nearly this steep we can argue that a diffuse component must exist with a density corresponding to ~100 Mpc interspacing of sources. This implies a lower limit on our neutrino flux above 10^{18} eV of $1.0/{\rm km^2 yr\,sr}$. This is pessimistically low. We obtained this result previously in Ref. 22, though we overestimated the detectability therein.

Our best two-component spectrum fit predicts

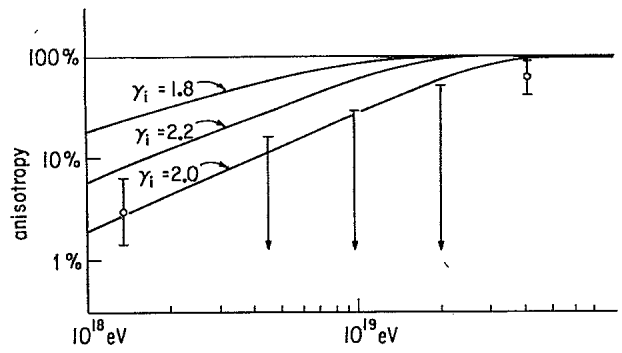

FIG. 13. The nucleon anisotropies of our three best fits are compared to the (large-error) data of Haverah Park. The best fit is $\gamma_i=2.0$ and seems to agree the best, though the errors are currently too large for this to be meaningful.

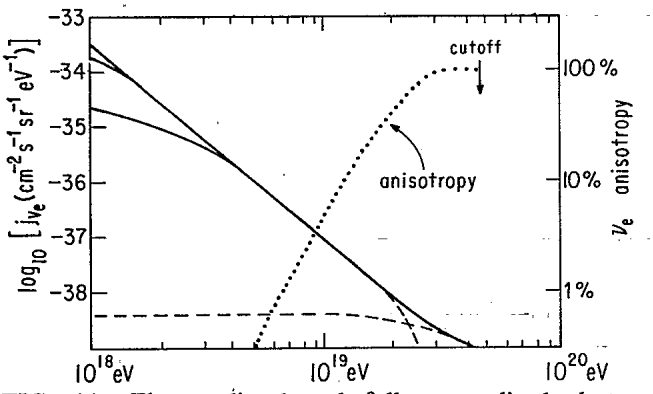

FIG. 14. The predicted and fully normalized electron-neutrino spectrum for our diffuse + semilocal model fit to the spectrum corresponding to injection index of 2.0. Note the occurrence of a neutrino anisotropy above 7×10^{18} eV, which is a much smaller effect than the nucleon anisotropy which begins at $\sim10^{18}$ eV due to the relatively large diffuse contribution here. The slope is 3.5 with $q_0=\frac{1}{2}$, and would differ slightly for other values. This spectrum is differential. The lower dashed curve is the Virgo component, and the UHE cutoff of the diffuse component is shown as the upper dashed curve.

$$I_{\nu_e}(10^{18})=0.652I_N(10^{18})$$
$$\sim1.65\times10^{-16}\ \mathrm{cm}^{-2}\mathrm{s}^{-1}\mathrm{sr}^{-1}$$

and this may be assumed to fall like $1/E^{2.5}$ up to $\sim10^{19}$ eV. Hence,

$$I_{\nu_e}(10^{19}\ \mathrm{eV})=5.22\times10^{-18}\ \mathrm{cm}^{-2}\mathrm{s}^{-1}\mathrm{sr}^{-1}\ ,$$

a result within two orders of magnitude of the Fly's Eye current upper limit for events above 10^{19} eV of 3.9×10^{-16} $\mathrm{cm}^{-2}\mathrm{s}^{-1}\mathrm{sr}^{-1}$. Of course, better would be a comparable limit for events above 10^{18} eV where our spectrum is more active by $300\times$. Such a limit may be possible with an improved analysis of the LPM effect in earth and a recalculation of the total neutrino cross section.

Previous estimates of the neutrino flux have been given by other authors to which we shall compare our present results. Stecker[28] has focused on the UHE limit of the spectrum and obtains results for assumed cosmic-ray spectra, but not including the assumed bright phase. These results can be compared to the dashed line of Fig. 14, the Virgo component for our two-component fit. Stecker's integrated normalizations for the low-energy (flat) end of the spectrum are $2\times10^{-17}\gtrsim I\gtrsim10^{-18}$ ($\mathrm{cm}^{-2}\mathrm{s}^{-1}\mathrm{sr}^{-1}$) compared to our Virgo component $I\sim10^{-19}$. The bright-phase result is clearly larger. For $\bar{z}=2$ we see that $I\sim10^{-15}$. If we neglected the bright phase but summed over sources out to the Hubble radius we would obtain results similar in magnitude to Stecker's. However, there is an important discrepancy in that Stecker's cutoff occurs at much higher energies for flatter injection spectra. This is a direct consequence of neglecting the transport effects which lead to a relatively universal cutoff energy.

Berezinsky[29] quotes fluxes from various sources other than photoproduction which fall below our results when extrapolated above 10^{18} eV. He also quotes a bright-phase result which gives roughly $I_{\nu_e}(10^{18}\ \mathrm{eV})\sim10^{-14}$. We are in good agreement with this (extrapolated) result, however we have assumed a power-law bright-phase parametrization while Berezinsky employs an exponential. We will be presenting elsewhere an exponential parametrization.[30]

The exciting possibility of observing the $I_{\nu_e}(10^{19}$ eV) result consistent with a $1/E^{2.0}$ injection spectrum is clear. It would constitute very strong evidence for the picture described here. Also, the eventual mapping of the spectrum down to lower energies where it should eventually roll over to a flat form at $\sim5\times10^{18}$ eV$/(1+\bar{z})^2$, would constitute a measurement of $\bar{z}$. Although we have not presently discussed it, departures of the neutrino slope from 3.5 in the present model contain information about the ubiquitous deceleration parameter q_0. In a future paper we will explore the cosmological possibilities further.[30]

Thus we see that a cosmological window may be opening here. We have assumed $q_0=\frac{1}{2}$ throughout, but a more general analysis is possible. We assume $\bar{z}$ large in our discussion. The quantities h_0 and m are also observables. With several orders of magnitude improvement in the data of this kind, such a model, if it survives, can in principle address the measurements of these quantities.

VI. RESULTS AND CONCLUSIONS

We have provided a detailed analysis of the spectral evolution upon passage through the 2.7°K microwave background and the effects of the cosmological Hubble expansion on the spectrum and corollary phenomena. Let us summarize our principle conclusions.

(i) The dominant effects in the long-range propagation and production of cosmic-ray nucleons are (a) photomeson production, (b) e^+e^- pair production, and (c) red-shifting of energy and bright-phase production. These effects should be treated in a transport formalism. Otherwise, important consequences such as the pile-up and dip will generally not appear. An injection spectrum with index will be steepened by the cumulative cosmological effects to an observed index of $\gamma_i/2+m/2-\frac{1}{4}$ for bright-phase parameter m. A pile-up of nucleons at about 4 to 7×10^{19} eV will occur followed by the conventional GZ cutoff. The pile-up shifts to lower energies due to the effects of pair production after 24 IL. A large dip appears at 10^{19} eV due to combined effects of pile-up and pair production.

(ii) The Haverah Park data has a statistically significant dip structure as well as the ankle. These are fit well by two-component models consisting of diffuse and semilocal parts, the latter when identified with the Virgo cluster gives excellent agreement with the reported anisotropy. We find that the $1/E^{2.0}$ injection spectrum gives the best statistical fit to the data. The result $R_{\mathrm{IC}}\sim100$ Mpc emerges from our fit to the data.

(iii) A potentially detectable electron-neutrino spectrum is predicted with a high-energy anisotropy slightly less well pronounced than the UHE nucleon anisotropy. Limits on the integrated neutrino flux above 10^{18} eV may soon rule out injection indices smaller than 1.5. The neutrino

spectrum has a universal slope of 3.5 up to 2×10^{19} eV, and a flattening below 5×10^{18} eV$/(1+\bar{z})^2$, and thus contains interesting information about the prequasar epoch, i.e., the "bright-phase maximum."

Most of our results are sufficiently general that they transcend the conclusions based upon the model fit. These methods will remain applicable to analyses of the spectrum as better and more data accrue.

ACKNOWLEDGMENTS

We wish to thank the following people for useful information discussions and encouragement throughout this lengthy project, about general aspects of cosmic-ray physics as well as points specific to this work: Professor J. Arafune, J. D. Bjorken, G. Cassiday, D. Cline, T. Gaisser, J. Linsley, J. Lloyd-Evans, E. Loh, C. Quigg, J. Rosner, P. Sololsky, T. Stanev, A. Watson, and G. Yodh.

[1]K. Greisen, Phys. Rev. Lett. **16**, 748 (1966); G. T. Zatsepin and V. A. Kuz'min, Pis'ma Zh. Eksp. Teor. Fiz. **4**, 114 (1966) [JETP Lett. **4**, 78 (1966)].

[2]F. W. Stecker, Phys. Rev. Lett. **21**, 1016 (1968); V. S. Berezinsky and G. T. Zatsepin, Yad. Fiz. **13**, 797 (1971) [Sov. J. Nucl. Phys. **13**, 453 (1971)]; V. S. Berezinsky, *ibid.* **11**, 399 (1979) [**11**, 222 (1979)]; V. S. Berezinsky, S. I. Grigoreva, and G. T. Zatsepin, Astrophys. Space Sci. **36**, 3 (1975).

[3]V. L. Ginzburg and S. I. Syrovatskii, *The Origin of Cosmic Rays* (Pergamon, Oxford, 1964); V. S. Berezinsky, in *Proceedings of the Fifteenth International Conference on Cosmic Rays, Plovdiv, 1977,* edited by B. Betev (Bulgarian Academy of Science, Plovdiv, Sofia, 1977), Vol. 10, p. 84.

[4]See the useful review of J. Linsley, in *Origin of Cosmic Rays,* edited by G. Setti, G. Spada, and A. Wolfendale (Reidel, Dordrecht, 1981), pp. 53—68 and references therein; also, A. M. Hillas, Phys. Rep. **20C**, 59 (1975).

[5]J. Lloyd-Evans and A. Watson, in *Proceedings of the 8th European Cosmic Ray Symposium, Bologna, 1983,* edited by G. Lucci *et al.* (Technoprint, Bologna, 1983), pp. 81—97.

[6]K. O. Theilheim and W. Langhoff, J. Phys. A **1**, 694 (1968); S. Karakula *et al., ibid.* **5**, 904 (1972).

[7]A. M. Hillas, Can. J. Phys. **46**, 5623 (1968).

[8]M. Giler, J. Wdowczyk, and A. Wolfendale, J. Phys. G **6**, 1561 (1980); A. Strong, J. Wdowczyk, and A. Wolfendale, J. Phys. A **7**, 120 (1974); **7**, 1767 (1974).

[9]G. Blumenthal, Phys. Rev. D **1**, 1596 (1970); see also E. Feenberg and H. Primakoff, Phys. Rev. **73**, 449 (1948).

[10]J. Puget, F. W. Stecker, and J. H. Bredekamp, Astrophys. J **205**, 638 (1976); V. S. Berezinsky, S. L. Grigor'eva, and G. T. Zatsepin, in *Proceedings of the Fourteenth International Conference on Cosmic Rays, Munich, 1975,* edited by Klaus Pinkau (Max-Planck-Institut, Munich, 1975), Vol. 2, p. 711.

[11]S. N. Ganguli and B. V Sreekantan, J. Math A **9**, No. 2 (1976); F. W. Stecker, Astrophys. Space Sci. **20**, 47 (1973).

[12]S. A. Bonometto, Lett. Nuovo Cimento **1**, 677 (1971); note the interesting possibility of cascades here. See also Stecker (Ref. 11), and J. Wdowcyzk *et al.* J. Phys. A **5**, 1419 (1972).

[13]J. Linsley, in *Proceedings of the Thirteenth International Conference on Cosmic Rays, Denver, 1973* (Colorado Associated University Press, Boulder, 1973), Vol. 5, p. 3207; and *Proceedings of the Fourteenth International Conference on Cosmic Rays, Munich, 1975* (Ref. 10), p. 598; also, in *18th International Cosmic Ray Conference, Bangalore, India, Conference Papers,* edited by N. Durgaprasad *et al.* (Tata Institute of Fundamental Research, Bombay, 1983).

[14]Haverah Park Collaboration (a) G. Cunningham *et al.*, Astrophys. J **236**, L71 (1980); (b) G. Brooke *et al.*, in *Sixteenth International Cosmic Ray Conference, Kyoto, 1979, Conference Papers* (Institute of Cosmic Ray Research, University of Tokyo, Tokyo, 1979), Vol. 8; J. Phys. A **6**, 47 (1973); contributions in *18th International Cosmic Ray Conference, Bangalore, India, Conference Papers* (Ref. 13), Vol. 4, p. 157.

[15]Yakutsk group: M. N. Dyankonov *et al.*, in *Sixteenth International Cosmic Ray Conference, Kyoto, 1979* (Ref. 14), Vol. 8, p. 168; D. D. Krasilnikov *et al.*, in *18th International Cosmic Ray Conference, Bangalore, India, Conference Papers* (Ref. 13), Vol. 4, p. 145.

[16]See L. Horton *et al.*, in *18th International Cosmic Ray Conference, Bangalore, India, Conference Papers* (Ref. 13), Vol. 4, p. 153, and references therein.

[17]J. Lloyd-Evans, A. Pollock, and A. Watson, in *Sixteenth International Cosmic Ray Conference, Kyoto, 1979, Conference Papers* (Ref. 14), Vol. 13, p. 130.

[18]A. Bower, *et al.*, J. Phys. G **9**, L53 (1983).

[19]C. T. Hill and D. N. Scramm, in *18th International Cosmic Ray Conference, Bangalore, India, Conference Papers* (Ref. 13); C. T. Hill and D. N. Schramm, Phys. Lett. **131B**, 247 (1983).

[20]F. W. Stecker, Comments Astrophys. **7**, 129 (1978); Astrophys. **228**, 919 (1979).

[21]Fly's Eye Experiment: in *18th International Cosmic Ray Conference, Bangalore, India, Conference Papers* (Ref. 13); for upward moving event limits see B. Cady *et al.*, University of Utah Report No. MN4-15 (unpublished) and P. Sokolsky, in Proceedings of the Cosmic Ray Workshop, Utah, 1983 (unpublished).

[22]A. Donnachie, in *Proceedings of the 1971 International Symposium on Electron and Photon Interactions at High Energies,* edited by N. B. Mistry (Laboratory of Nuclear Studies, Cornell University, Ithaca, NY, 1972); also T. A. Armstrong *et al.*, Phys. Rev. D **5**, 1640 (1972).

[23]H. Genzel and W. Pfeil, Bonn University Report No. PI B1-168, 1972 (unpublished).

[24]S. Weinberg, *Gravitation and Cosmology* (Wiley, New York, 1972).

[25]V. Berezinsky and G. T. Zatsepin, Yad. Fiz. **11**, 111 (1970) [Sov. J. Nucl. Phys. **11**, 61 (1970)]; V. S. Berezinsky and V. L. Ginzburg, in *Proceedings of the 1980 DUMAND Symposium, Honolulu,* edited by V. J. Stenger (Hawaii DUMAND Center, Honolulu, 1981), Vol. 2, p. 181; V. S. Berezinsky and L. M. Ozernoi, *ibid.*, Vol. 2. p. 202; V. S. Berezinsky, in *Proceedings of the 1978 DUMAND Summer Workshop, La Jolla, California,* edited by A. Roberts (Scripps Institute of Oceanography, La Jolla, 1979), Vol. 2, p. 155; F. W. Stecker, in *Neutrino '79,* proceedings of the International Conference on Neutrinos, Weak Interactions, and Cosmology, Bergen, Norway, 1979, edited by A. Haatuft and C. Jarlskog (University of Bergen, Bergen, 1980), Vol. 2, p. 475; R. B. Partridge and P. J. E. Peebbles, Astrophys. J. **147**, 868 (1967).

[26]M. Schmidt, in *Stars and Stellar Systems,* edited by G. Kuiper (University of Chicago Press, 1975), Vol. IX.

[27]M. S. Longair, Mon. Not. R. Astrophys. Soc. **133**, 421 (1966).

[28]Stecker, Ref. 20; S. H. Margolis, D. N. Schramm, and R. Silberger, Astrophys. J. **221**, 990 (1978).

[29]V. S. Berezinsky, in *Proceedings of the 1978 DUMAND Summer Workshop, La Jolla, California* (Ref. 25), Vol. 2, p. 155.

[30]C. T. Hill and G. Perez (in preparation).